Targeting the redox vulnerability of acute myeloid leukaemia cells with a combination of auranofin and vitamin C

Zhiliang Hei, Shujun Yang, Guifang Ouyang, Jolimar Hanna, Michel Lepoivre, Tony Huynh, Lorea Aguinaga, Bruno Cassinat, Nabih Maslah, Marie-Pierre Golinelli, et al.

Title: Targeting the redox vulnerability of acute myeloid leukaemia cells with a combination of auranofin and vitamin C

Zhiliang Hei[1], Shujun Yang[2], Guifang Ouyang[2], Jolimar Hanna[1], Michel Lepoivre[1], Tony Huynh[3], Lorea Aguinaga[3], Bruno Cassinat[4], Nabih Maslah[4], Mickaël Bourge[5], Marie-Pierre Golinelli-Cohen[1], Olivier Guittet[1], Cindy Vallières[1], Laurence Vernis[1], Pierre Fenaux[3], Meng-Er Huang[1]

[1] Université Paris-Saclay, Institut de Chimie des Substances Naturelles, CNRS UPR 2301, 91198 Gif-sur-Yvette, France.
[2] Department of Hematology, The First Affiliated Hospital of Ningbo University, Ningbo, Zhejiang, China.
[3] Service d'Hématologie Séniors, Hôpital Saint-Louis, Assistance Publique-Hôpitaux de Paris, Université de Paris Cité, 75010 Paris, France.
[4] INSERM UMR 1131, Université Paris Cite, Hôpital Saint-Louis, IRSL, 75010 Paris, France.
[5] Cytometry Facility, Imagerie-Gif, Université Paris-Saclay, CEA, CNRS, Institute for Integrative Biology of the Cell (I2BC), 91198 Gif-sur-Yvette, France.

Running Title: **Targeting the redox vulnerability of AML cells**

Correspondence:

Pierre Fenaux, Service d'Hématologie Séniors, Hôpital Saint-Louis, 75010 Paris, France.
email: pierre.fenaux@aphp.fr

Meng-Er Huang, CNRS UPR 2301, Institut de Chimie des Substances Naturelles, Bâtiment 27, 1 avenue de la Terrasse, 91198 Gif-sur-Yvette, France.
Phone: 33-1-69823776; e-mail: meng-er.huang@cnrs.fr

Summary

Acute myeloid leukaemia (AML) is a heterogeneous disease characterized by complex molecular and cytogenetic abnormalities. Pro-oxidant cellular redox status is a common hallmark of AML cells, providing a rationale for redox-based anticancer strategy. We previously discovered that auranofin (AUF), initially used for the treatment of rheumatoid arthritis and repositioned for its anticancer activity, can synergize with a pharmacological concentration of vitamin C (VC) against breast cancer cell line models. In this study, we observed that this drug combination synergistically and efficiently killed cells of leukemic cell lines established from different myeloid subtypes. In addition to an induced elevation of reactive oxygen species and ATP depletion, a rapid dephosphorylation of 4E-BP1 and p70S6K, together with a strong inhibition of protein synthesis were early events in response to AUF/VC treatment, suggesting their implication in AUF/VC-induced cytotoxicity. Importantly, a study on 22 primary AML specimens from various AML subtypes showed that AUF/VC combinations at pharmacologically achievable concentrations were effective to eradicate primary leukemic $CD34^+$ cells from the majority of these samples, while being less toxic to normal cord blood $CD34^+$ cells. Our findings indicate that targeting the redox vulnerability of AML with AUF/VC combinations could present a potential anti-AML therapeutic approach.

Keywords: auranofin, vitamin C, oxidative stress, acute myeloid leukaemia.

INTRODUCTION

Acute myeloid leukaemia (AML) is a genetically heterogeneous haematopoietic malignancy characterized by the proliferation and accumulation of myeloid blast cells in the bone marrow and peripheral blood. Among all subtypes of AML assigned according to classical morphologically-based French-American-British (FAB) classification, only acute promyelocytic leukaemia (type M3) can be effectively treated with all-trans retinoic acid and arsenic trioxide. For the remaining AML subtypes, relapse remains a major challenge.[1-3] Recently, targeted therapies against AML have been intensively investigated.[4,5] However, despite encouraging results, the majority of AML patients treated with available target therapies eventually relapse. Indeed, AML originates from haematopoietic stem/progenitor cells with many oncogenic drivers.[6,7] A patient may further harbor a mosaic of genetically distinct subclonal leukemic populations, which creates a challenging scenario for precision therapy directed toward specific genetic alterations. Therefore, novel treatments broadly targeting blasts and more primitive leukemic cells without severely affecting normal haematopoietic cells are highly desired.

Defects in reactive oxygen species (ROS) homeostasis and redox signaling perturbation are at the crux of many pathological processes. One of the significant features of cancer cells, including leukemic cells, when compared to their normal counterparts, is a persistent pro-oxidative state due to cellular events such as activation of oncogenes, aberrant metabolic stress and mitochondrial dysfunction.[8-11] Therefore, malignant cells would be more vulnerable to further oxidative insults than their normal counterparts, providing a selective window to induce preferential cancer cell death by a ROS-mediated mechanism. Among several druggable redox-based molecules, auranofin (Ridaura, AUF) has received particular attention. AUF is an orally administered, gold (Au)-containing compound that was approved by the US FDA (Food and Drug Administration) in 1985 for treatment of rheumatoid arthritis. Interestingly, AUF has

emerged as a potential candidate for multiple repurposed therapies including cancers.[12] Clinical trials of AUF in chronic lymphocytic leukaemia, ovarian cancer and other solid tumors have been carried out or still ongoing.[13] A proposed central mechanism for its anticancer activity is the inhibition of thioredoxin reductases.[12,14,15] AUF has also been reported to target the proteasome,[16] induce endoplasmic reticulum stress,[17] inhibit several tumor-signaling pathways and disrupt actin filaments.[18-21] In an effort to identify rational drug combinations that enhance AUF anticancer activity, we discovered that the AUF and vitamin C (VC, ascorbic acid) combination exerts a synergistic and H_2O_2-mediated cytotoxicity towards the triple-negative breast cancer cell line MDA-MB-231 in culture and in mouse xenografts.[22] VC is a natural antioxidant that becomes a ROS-generating molecule at high pharmacological doses.[23] The mechanisms for VC-induced cytotoxicity are related to H_2O_2 generation, depletion of reduced glutathione and others.[24-27] In this study, we found that the AUF/VC combination exerted a strong synergy in killing several myeloid leukaemia cell lines. In addition to intracellular ROS elevation and ATP depletion, dephosphorylation of 4E-BP1 (eukaryotic translation initiation factor 4E-binding protein 1) and p70S6K (p70S6 kinase), and drastic protein synthesis arrest occurred in few hours in response to AUF/VC treatment. Importantly, AUF/VC combinations at pharmacologically relevant concentrations were effective to kill most primary leukemic $CD34^+$ cells from several types of AML patients while being less toxic to normal cord blood $CD34^+$ cells, suggesting a potentially straightforward anti-leukemic application.

MATERIALS AND METHODS

Cell lines and reagents, oxidative stress assessment, intracellular ATP content analysis and mitochondrial membrane potential (MMP) measurement, western blotting and redox western blotting, as well as detailed descriptions for cell death assessment, global nascent protein

translation measurement, and analysis of primary AML samples and normal cord blood specimens are presented in the Supplementary Materials and Methods section.

Cell death assessment for cells from cell lines

Cells were seeded in 6-well plates at a density of 2×10^5 cells per ml for overnight incubation and subjected to treatments for 48 h. Cells were then harvested, washed in PBS containing 1% fetal bovine serum (FBS) and resuspended in an equal volume of PBS/1% FBS/propidium iodide (PI, 1 µg/ml) before being analyzed by a Cytoflex S flow cytometer (Beckman Coulter-France, Villepinte). Combined drug effects were analyzed by the Chou-Talalay method using CompuSyn software.[28] Drug synergistic, additive, and antagonistic effects are defined by combination index (CI) values of < 0.9, 0.9–1.1, and > 1.1, respectively. Drugs-induced cell death of leukemia cells in co-culture with HS-5 bone marrow stromal cell line was assessed following the experimental setup described by Podszywalow-Bartnicka *et al*.[29]

Global nascent protein translation measurement

Protein Synthesis Assay Kit (ab239725, Abcam) based on O-Propargyl-puromycin was used for the detection of global nascent proteins of treated cells following the instructions of the manufacturer. Cycloheximide was used as a control for protein translation inhibition. Nascent polypeptides synthesis was detected with a Cytoflex S flow cytometer using the FITC channel. Results were analyzed and displayed using Kaluza software.

Primary AML samples and normal haematopoietic specimens

Peripheral blood or bone marrow samples from 22 AML patients were used in this study. The clinical data of these patients are detailed in Supplementary Table S1. AML samples (AML_1-16) and umbilical cord blood cells from Hôpital Saint-Louis (Paris, France) were obtained from

donors after informed consent and in compliance with the Declaration of Helsinki. AML samples (AML_17-22) from the Department of Hematology of The First Affiliated Hospital of Ningbo University (Ningbo, China) were obtained after informed consent of the donors, and the study was approved by the Ethics Committee of The First Affiliated Hospital of Ningbo University and was in accordance with the Declaration of Helsinki. A detailed description on mononuclear cell isolation, culture, treatment and analysis is included in the Supplementary Materials and Methods section. After drug treatment for 48 h or 72 h, cells were harvested, washed with PBS, and resuspended in 100 µl of PBS/1% FBS containing 1X brilliant stain buffer plus. The cells were then incubated in the presence or absence of CD34-APC and CD38-PE antibodies for 30 min. Once washed with PBS, the cells were resuspended in an equal volume of PBS containing 1% FBS and 1 µM Sytox Blue and analyzed by a Cytoflex S flow cytometer or a FACSCanto flow cytometer (Becton Dickinson-China, Shanghai). For each sample, the maximum number of events were collected. Sytox Blue staining was used to discriminate dead cells. Live $CD34^+$ cells ($CD34^+$ Sytox $Blue^-$) were gated and scored. Results were analyzed and displayed using Kaluza software.

Statistical Analysis

Data were presented as the mean ± standard deviation (SD). Whenever necessary, an unpaired, two tailed *t* test with Welch's correction available in the GraphPad Prism 8 software was performed to compare the difference between two groups, and ordinary one-way ANOVA (multiple comparisons) was used to estimate the differences for differently treated cells. Significance was accepted with $p < 0.05$.

RESULTS

AUF and VC combinations synergistically kill myeloid leukaemia cells from various cell lines

To determine whether AUF and VC display synergistic antileukemic activity, Kasumi-3, KG-1, Kasumi-1, NB-4, HL-60 and K562 cells, all derived from heterogeneous myeloid leukaemia subtypes, were treated with drug combinations and corresponding single-drugs (Figure 1). Different cell lines displayed different sensitivity to AUF or VC. Interestingly, upon treatment with AUF 0.25 μM/VC 0.25 mM, cell death was significantly enhanced compared with AUF or VC alone in all cell lines tested, while treatment with AUF 0.5 μM/VC 0.5 mM killed almost all cell line cells. Synergistic cell death induction as indicated by CI values was observed in all 6 cell lines under combination treatments and high synergy with low CI values was also notable in several situations (Figure 1A). Because stromal cells and bone marrow environment play a major role in promoting resistance to chemotherapy, we evaluated the effects of HS-5 cells on AUF/VC-induced cell death. KG-1 and K562 cells were moderately but significantly less sensitive to AUF 0.5 μM/VC 0.5 mM-induced cell death when co-cultured with HS-5 cells as compared to mono-culture conditions, with viable cells 17.4 ± 4.8% versus 0.2 ± 0.5% for KG-1 cells and 14.2 ± 8.4% versus 5.3 ± 2.7% for K562 cells (Figure 1A, 1B). Nevertheless, AUF 0.5 μM/VC 0.5 mM combination remained highly efficient to kill KG-1 and K562 cells without substantial toxicity to stromal cell line (Figure 1B). Taken together, these data demonstrate a large spectrum and synergistic anti-AML activity of AUF/VC combinations. For most of the experiments described below, we used the combination AUF 0.5 μM/VC 0.5 mM in KG-1 and K562, two highly used cells lines. K562, established from a chronic myeloid leukaemia at blast crisis, has been known to be resistant to many chemotherapeutic molecules.

ROS increase, endogenous protein oxidation, ATP depletion and MMP loss are early events induced by AUF/VC combination

We used carboxy-H_2DCFDA and MitoSOX Red to detect global intracellular and mitochondrial ROS levels respectively (Figure 2A). In KG-1 cells treated for 2 h with the AUF 0.5 μM/VC 0.5 mM, signals for DCF (the oxidation product of carboxy-H_2DCFDA) moderately increased compared to AUF- or VC-treated cells, while MitoSOX signals were more markedly elevated with the drug combination. Similarly, for K562 cells, only a combination treatment caused an increase in MitoSOX and DCF signals. As carboxy-H_2DCFDA and MitoSOX Red are two chemical ROS sensors with different specificities and dynamics, we further assessed the redox state of cytosolic PRDX1 and mitochondria-localized PRDX3 (Figure 2B, 2C). A ratio of dimeric PRDX1 or PRDX3 (oxidized form) to its total protein (oxidized plus reduced monomeric forms) reflects respective redox environment in the cytosol and mitochondria. In KG-1 and K562 cells, combination treatments increased PRDX1 and PRDX3 oxidation within 2 h and further enhanced at 4 h, indicating that ROS levels increased both in the cytosol and in mitochondria.

Next, we explored whether AUF, VC and AUF/VC affected cellular ATP content. During a time course study ranging from 2 to 8 h after addition of the drug(s), AUF had no effect while VC had moderate effects from 4 h treatments, whereas AUF/VC induced rapid and significant ATP decline compared to VC in KG-1 and K562 cells (Figure 3A). Measurements in Kasumi-3 and HL-60 cells also confirmed this observation and revealed different dynamics of ATP reduction in 4 cell lines in response to drug treatments (Figure 3A, Supplementary Figure S1). As ATP level, MMP is an important parameter of mitochondrial function and an indicator of cell health. The cell-permeant ratiometric JC-1 sensor was used to evaluate the MMP in K562 cells (Figure 3B). After AUF/VC treatment for 4 h, more than half of the cells experienced MMP loss. Taking these observations together, we concluded that AUF/VC treatments increase ROS accumulation, reduce the MMP, and inhibit intracellular ATP synthesis.

Implication of mTOR cell signaling pathway in response to AUF/VC treatments

Implication of mTOR (mammalian target of rapamycin) pathway in the mechanisms of action of AUF or VC as single agent has been reported.[30,31] Because this pathway plays a role in cell proliferation, cell death and chemoresistance, we thus studied primarily the phosphorylation status of several key actors of the mTOR pathway, including 4E-BP1, p70S6K, mTOR and AKT, in response to AUF, VC, or AUF/VC treatments. High levels of phosphorylated 4E-BP1 (p-4E-BP1) and consequent enhanced protein translation activity were reported in human cancers.[32] Indeed, p-4E-BP1 (Thr37/46) in both non-treated KG-1 and K562 cells were high (Figure 4A). Remarkably, a rapid, significant and progressive decrease of p-4E-BP1 (Thr37/46) was detected after AUF/VC treatment in KG-1 and K562 cells while total 4E-BP1 levels were unchanged or even increased (Figure 4A). Dephosphorylation of 4E-BP1 was also clearly visible in Kasumi-3 and HL-60 cells at 4 h treatment (Supplementary Figure S2). A decrease of phosphorylated p70S6K (p-p70S6K, Thr389) was also detected as early as 2 h of treatment (Figure 4B). Both 4E-BP1 and p70S6K are downstream effectors of mTOR complex 1 (mTORC1), their dephosphorylation may suggest an inhibition of mTORC1 activity. However, there was only a moderate decrease of phosphorylated mTOR (p-mTOR, Ser2448) at 2 h and 4 h after treatment with the combination (Figure 4C). We also detected a sharp and temporary rise of phosphorylated AKT (p-AKT, Ser473) in AUF/VC treated cells at 2 h, while total AKT levels were unchanged (Figure 4D). Phosphorylation of AKT (Ser473) is generally considered as an indicator of mTOR complex 2 (mTORC2) activation. The contrast between the dephosphorylation of 4E-BP1 and p70S6K and that of mTOR may suggest a possible mechanism triggering dephosphorylation of 4E-BP1 and p70S6K independent of mTOR inhibition. Consistent with this possibility, the mTORC1 activator MHY1485 at concentrations

that enhanced 4E-BP1 phosphorylation failed to suppress AUF/VC-induced 4E-BP1 dephosphorylation (Figure 4E).

This dramatic and rapid dephosphorylation of 4E-BP1 and p70S6K strongly suggests that AUF/VC combinations can affect protein translation. Indeed, AUF/VC-induced inhibition of global protein synthesis was evident at 2 h treatment in both KG-1 and K562 cells (Figure 5). At 4 h, its effectiveness was comparable to that of cycloheximide, known as a strong protein synthesis inhibitor, while the corresponding single drug treatments had only limited effects. Therefore, AUF and VC had a synergistic inhibitory effect on global protein synthesis. Taken together, these mechanistic investigations reveal that AUF/VC combinations cause a rapid and strong dephosphorylation of 4E-BP1 and p70S6K, and an inhibition of protein synthesis. This could be one of the mechanisms leading to rapid leukemic cell death induced by AUF/VC.

AUF/VC combinations efficiently kill primary AML CD34$^+$ cells but are less toxic to normal CD34$^+$ haematopoietic cells

To measure drug responses in primary AML cells, we tested 22 AML samples collected from patients at diagnosis or under treatments. These 22 AML specimens, 16 of peripheral blood and 6 of bone marrow, had different molecular and clinical characteristics, thus representing a reasonable spectrum of AML subtypes (Table S1). Treatment effect was measured on the CD34$^+$ population which includes AML blasts, progenitor cells and a small set of leukaemia stem cells (LSCs) in most of the cases. Of note, CD34$^+$ cells are absent in normal human peripheral blood at physiological situation, and CD34$^+$ cells enriched in mononuclear cells from AML patient blood are exclusively leukemic. CD34$^+$ cells from AML bone marrow should contain a very small but negligible set of healthy CD34$^+$ cells, as isolated mononuclear cells from AML samples were predominantly leukemic blasts. Therefore, CD34$^+$ cells from these samples globally represent a leukemic cell population. We initially designed our flow cytometry

measurements to further gate and score the $CD34^+$ $CD38^-$ fraction that is enriched for LSCs. However, due to limited sample volumes in most specimens, detection and evaluation of $CD34^+$ $CD38^-$ cells were not reliable and not included in our final analysis.

We treated isolated mononuclear cells from patient peripheral blood or bone marrow with AUF 0.5 μM, VC 0.5 mM and their combination, as a first choice. When the cell number permitted, the conditions AUF 0.25 μM, VC 0.25 mM and/or AUF 1 μM, and VC 1 mM and their corresponding combinations were also employed. The gating strategy of cell populations is outlined in Supplementary Figure S3. The $CD34^+$ Sytox $Blue^-$ population was used as the standard gate for live AML immature cells and its density (events/μl) after 48 h or 72 h of treatment was determined. A typical example of flow cytometry analysis with an AML sample following AUF, VC and combination treatments is presented in Figure 6A and a total of 22 samples were analyzed (Table 1). Among them, AML_4 did not contain any distinct $CD34^+$ population (Supplementary Figure S4) and was excluded from further study. It is known that a small proportion of AML patients has no AML $CD34^+$ population.[33,34] There were considerable inter-patient differences in $CD34^+$ cell sensitivity to AUF or VC single-drug treatment (Table 1, Figure 6B). $CD34^+$ cells from AML_7, 10, 17, 18 were sensitive to AUF 0.5 μM (>80 % cell death), while $CD34^+$ from AML_11, 14, 15, 16, 18 were sensitive to VC 0.5 mM. Remarkably, the combination AUF 0.5 μM/VC 0.5 mM killed AML $CD34^+$ cells efficiently (>80% cell death) in the majority of the AML samples (19/21) with the exception of those from AML_5 and AML_19. The combination AUF 1 μM/VC 1 mM eliminated >98% AML $CD34^+$ except those from AML_5 and AML_19 who still had 18.4% and 28.2% of survival cells, respectively (Table 1). Among the 8 samples tested with the AUF 0.25 μM/VC 0.25 mM combination, 5 of them displayed high sensitivity (>80% cell death, Table 1). Taken together, these data indicate that AUF/VC combinations at pharmacological achievable concentrations are highly effective in killing a large spectrum of AML premature cells. As dephosphorylation of 4E-BP1 was a

common trait observed in leukemia cell lines in response to AUF/VC treatment (Figure 4A, Supplementary Figure S2), we analyzed the phosphorylation levels of 4E-BP1 in $CD34^+$-enriched primary leukaemia cells from AML_6 and AML_16 in response to AUF 0.5 μM, VC 0.5 mM and AUF 0.5 μM/VC 0.5 mM treatments. High level of p-4E-BP1 (Thr37/46) underwent remarkable dephosphorylation 4 h after treatment with the combination in both samples (Figure 6C).

In order to evaluate the toxicity of AUF, VC and their combinations to normal haematopoietic cells, 5 samples of cord blood cells were analyzed (Figure 6D). Healthy $CD34^+$ cells showed significantly lower sensitivity to AUF, VC or AUF/VC combinations compared to most cases of AML cells (19/21, AML_4, 5, 19 were not included) when treated under the same conditions (Figure 6E). The $CD34^+$ cells from AML_5 and AML_19, although more resistant to single and combination treatments than other AML samples, were still responsive to AUF 0.5 μM/VC 0.5 mM and AUF 1 μM/VC 1 mM treatments (Table 1). These comparisons suggest a potential therapeutic window for the selective targeting of a large proportion of AML cases.

AUF/VC combination efficiently inhibits colony-formation capacity of AML cells

To further characterize the AUF/VC effect on the clonogenic capacities of AML cells, we performed methylcellulose colony-forming unit (CFU) assays. As illustrated in Figure 7A, in 5 AML samples tested, AUF 0.5 μM or VC 0.5 mM treatment moderately reduced the ability of primary AML cells to form colonies with large inter-sample differences, while AUF/VC combination had a drastic effect on CFU inhibition, reducing both CFU number and colony size. In contrast, the same combination displayed less toxicity on CFU from cord blood samples. CFU assay confirmed that AUF/VC combinations have a potent activity against AML stem/progenitor cells while sparing part of normal haematopoietic counterparts.

DISCUSSION

Anticancer activity and mechanism of action of AUF and VC as individual molecules have been the subjects of many studies. Both molecules reveal a complex and multifactorial mode of action that could be partially cancer cell type- or drug dose-dependent.[12,13,23] To our knowledge, no real mechanistic study has been published since our publication describing the identification of this combination in breast cancer cells.[22] A synergistical ROS accumulation appeared to be one of the predominant early events,[22,35] but whether AUF and VC synergy simply resulted from enhanced ROS accumulation, following VC-mediated ROS generation coupled with AUF-mediated TrxR inhibition, or from combined action affecting multiple targets remained unknown. In our current leukemic models, AUF and VC synergy was reflected by global and mitochondrial ROS elevation, ATP depletion, MMP loss, dephosphorylation of 4E-BP1 and p70S6K, and protein synthesis inhibition which all occurred very early following AUF/VC treatments. Cells treated with AUF or VC alone (at the same concentrations) did not display such effects.

We focused on the mTOR pathway as both AUF and VC single-drug treatments have been reported to have an impact on this pathway in cell models other than leukemic cells.[30,31] The core elements of the mTOR pathway are increasingly considered as interesting anticancer targets.[36] A proteomic analysis revealed that AUF (0.5 µM) inhibited expression and/or phosphorylation of several key actors, including S6, 4E-BP1, Rictor, p70S6K, mTOR, TSC2, AKT and GSK3 in two non-small cell lung cancer cell lines. Most of those inhibitions occurred at 8 h and were more dramatic at 24 h.[30] On the other hand, pharmacological concentration of VC (at 0.5 to 1 mM) affected both the mTORC1 and mTORC2 in a dose-dependent manner at 2 h in a variety of solid tumor cell lines.[31] VC promoted Rictor ubiquitination and degradation and upregulated the expression of HMOX1, both involved in VC-induced mTOR pathway

inhibition. Furthermore, effects of VC on inhibiting cell viability was blocked by MHY1485, the activator of mTORC1, or by TSC2 knockdown, which leads to constitutively active mTOR. In our current study, a decrease in the phosphorylation levels of 4E-BP1 and p70S6K and in protein synthesis was clearly visible after 2 h exposure to AUF/VC and further accentuated at 4 h, but this was not the case in the corresponding single-drug treated KG-1 and K562 cells. mTOR phosphorylation was only moderately reduced. Conversely, we observed a dramatic rise of p-AKT at 2 h which was attenuated at 4 h, suggesting a temporary mTORC2 activation. These data indicate an implication of several core elements of mTOR pathway in response to AUF/VC that may potently affect multiple sites of the mTOR axis and even beyond. In fact, AUF/VC-induced strong dephosphorylation of 4E-BP1 and p70S6K, rapid protein synthesis arrest and cell death were far greater than those caused by the allosteric mTORC1 inhibitor rapamycin or mTOR active-site inhibitors Torin1[37,38] (data not shown). In line with these results, we found that neither AUF/VC-induced 4E-BP1 dephosphorylation nor cell death could be blocked by MHY1485 (Figure 4E, data not shown). Therefore, an implication of other mechanisms leading to strong dephosphorylation of 4E-BP1 and p70S6K, and rapid protein synthesis arrest independent of the classic mTOR axis is highly possible. We will thus further explore implication of other kinases, phosphatases or endoplasmic reticulum stress pathway, as reported in literature.[32,39,40]

AUF and VC combinations produced a synergistic effect on myeloid leukemic cells from different origins *in vitro*. AUF 0.25 μM/VC 0.25 mM was able to reach IC50 while AUF 0.5 μM/VC 0.5 mM was able to kill almost all leukemic cells. The presence of HS-5 stromal cells, which are broadly used in co-culture experiments mimicking the bone marrow microenvironment,[29,41,42] could moderately attenuate AUF/VC-induced toxicity to leukemia cells. This commonly observed protective effect is attributed to characteristics of HS-5 cells that provide growth and survival signals, thereby promoting the development of drug resistance.

Nevertheless, AUF/VC combinations remained highly effective to kill leukemia cells with much less toxicity to HS-5 cells. Similarly, even though there was a large disparity in sensitivity of different AML samples to AUF or VC, most of them were highly sensitive to AUF 0.5 μM/VC 0.5 mM. Therefore, AUF/VC combinations can largely increase anti-AML spectrum and decrease dosage of each single drug to achieve the same efficacy. These *in vitro* drug concentrations are pharmacologically and clinically relevant. Plasma AUF concentrations of approximately 1–2 μM are achievable with tolerable side effects in patients or volunteer subjects who receive the recommended dose for rheumatoid arthritis, typically 6 mg/day.[13,43] On the other hand, plasma VC concentrations greater than 10 mM are achievable in humans by intravenous administration and are well tolerated.[23]

Side effects caused by the risk of indiscriminate attacks of excessive drug-induced ROS on normal tissues are considered as the main concern for the redox-based anticancer strategy.[44] For the AUF and VC combinations, several evidences strongly suggest a reasonable selective therapeutic window. First, three AUF/VC combinations tested in our study displayed higher toxicity to most AML $CD34^+$ cells while sparing a significantly higher proportion of normal haematopoietic counterparts in flow cytometry-based assays. Secondly, Graczyk-Jarzynka *et al* also observed that an efficient AUF/VC combination against malignant B cells, using drug concentrations similar to the ones we employed, resulted in mild toxicity to normal peripheral blood B-cells and no toxicity to centroblasts cultured *ex vivo*.[35] Thirdly, we previously found that two AUF/VC combinations of different concentrations that resulted in rapid regression of MDA-MB-231 cell xenograft did not cause detectable haematological abnormality in mice during treatment.[22] Although we had no knowledge of AUF and VC concentrations in mouse blood, *in vitro* drug combinations required for efficient killing of MDA-MB-231 cells were higher than what we employed for AML cells.[22] It should also be possible to identify optimal AUF/VC combinations with better synergy against leukemic cells and less toxicity to normal

cells by testing various concentrations of AUF and VC. Our data show a broad susceptibility of various leukemic cell lines as well as primary AML samples to AUF/VC combinations. A further study with a larger set of samples could help to identify a highly sensitive subset that are especially suitable to AUF/VC-based therapy and to identify potential predictive biomarkers, thus increasing the selective therapeutic window. In practice, a simple flow cytometry-based *in vitro* assay as we performed in this study may reflects an *in vivo* situation to some extent and help to select candidates for such treatment.

Drug-resistant LSCs are thought to be responsible for relapse after initial successful eradication of the bulk AML cell population.[7] The specific elimination of LSCs, while sparing the healthy normal haematopoietic stem cells, is one of the major challenges in the AML treatment. We were not able to determine the effect of AUF/VC on the LSCs-enriched $CD34^+$ $CD38^-$ population due to limited amount of samples. However, the very radical elimination of AML $CD34^+$ population (usually >98% after one-shot treatment with AUF 0.5 μM/VC 0.5 mM) suggests its capacity to eradicate primitive AML cells. CFU assays provide another indication that the AUF/VC combination could be efficient against AML stem/progenitors cells. Additional studies are needed to fully confirm that AUF/VC is indeed capable of efficiently targeting LSCs, while sparing the normal haematopoietic stem cells.

Our present study demonstrated that AUF/VC combinations at pharmacologically relevant concentrations were able to synergistically and efficiently kill cells of leukemic cell lines established from different myeloid subtypes and to eliminate most primary leukemic $CD34^+$ cells from several types of AML patients while being less toxic to normal cord blood $CD34^+$ cells. Mechanistically, a rapid and strong dephosphorylation of 4E-BP1 and p70S6K, and a consequent strong and sustained inhibition of protein synthesis could implicate in AUF/VC-induced cytotoxicity. AUF and VC are both FDA-approved drugs with documented pharmacokinetic and safety profiles in humans. AUF and VC combination may provide a new

anti-AML strategy, with higher specificity against AML cells than conventional chemotherapy, and broader and more efficient activity than target therapies. Furthermore, the redox-based mechanisms of these drugs may overcome drug resistance induced in other therapy regimens, and thereby provide novel therapeutic opportunities.

AUTHOR CONTRIBUTIONS

PF and MEH conceived the study. ZH and MEH designed the strategy and methodology. MEH supervised the project. ZH, SY, JH and MEH carried out experiments. GO, TH, LA, BC, NM and PF provided AML samples, cord blood samples and clinical data, MB helped with the cytometry analysis. GO, ML, BC, NM, MPGC, OG, CV, LV provided reagents and critical inputs. All authors participated in data analysis and interpretation. ZH and MEH wrote the original draft. All authors were involved in the review and editing of the manuscript.

ACKNOWLEDGMENTS

We thank Christine Chomienne (Hôpital Saint-Louis, Paris) for KG-1, K562 and NB-4 cell lines. The present work has benefited from Imagerie-Gif core facility supported by l'Agence Nationale de la Recherche (ANR-11-EQPX-0029/Morphoscope, ANR-10-INBS-04/FranceBioImaging, ANR-11-IDEX-0003-02/ Saclay Plant Sciences) (Karine Madiona, Romain Le Bars and Sandrine Lecart).

FUNDING INFORMATION

This work was supported by the Centre National de la Recherche Scientifique (CNRS) and the Institut de Chimie des Substances Naturelles. This work was also supported by a specific funding from the Association Laurette Fugain (ALF 2020/02). Zhiliang Hei is supported by a

PhD fellowship from the China Scholarship Council. Jolimar Hanna is supported by a PhD program from the Paris-Saclay University. Laurence Vernis is supported by INSERM.

CONFLICT OF INTEREST STATEMENT

There is no conflict of interest by any of the authors.

DATA AVAILABILITY STATEMENT

All data and protocols in the current study are available from the corresponding authors upon request.

ETHICS STATEMENT

The study has been approved by the local Ethics committee in compliance with the Declaration of Helsinki. All patients gave specific informed consent for the use of surplus tissue.

PERMISSION TO REPRODUCE MATERIAL FROM OTHER SOURCES

n/a

CLINICAL TRIAL REGISTRATION

n/a

ORCID

Pierre Fenaux : https://orcid.org/0000-0002-0468-3553

Meng-Er Huang: https://orcid.org/0000-0002-9312-4760

SUPPLEMENTARY INFORMATION

Supplementary Materials and Methods

Supplementary Table S1

Supplementary Figure S1, Figure S2, Figure S3, Figure 4S

REFERENCES

1. Kantarjian H, Kadia T, DiNardo C, Daver N, Borthakur G, Jabbour E, et al. Acute myeloid leukemia: current progress and future directions. Blood Cancer J. 2021. 11(2):41.
2. Jaramillo S, Schlenk RF. Update on current treatments for adult acute myeloid leukemia: to treat acute myeloid leukemia intensively or non-intensively? That is the question. Haematologica. 2023. 108(2):342-352.
3. Stubbins RJ, Francis A, Kuchenbauer F, Sanford D. Management of Acute Myeloid Leukemia: A Review for General Practitioners in Oncology. Curr Oncol. 2022. 29(9):6245-6259.
4. Kayser S, Levis MJ. Updates on targeted therapies for acute myeloid leukaemia. Br J Haematol. 2022. 196(2):316-328.
5. Bhansali RS, Pratz KW, Lai C. Recent advances in targeted therapies in acute myeloid leukemia. J Hematol Oncol. 2023. 16(1):29.
6. Thomas D, Majeti R. Biology and relevance of human acute myeloid leukemia stem cells. Blood. 2017. 129(12):1577-1585.
7. van Gils N, Denkers F, Smit L. Escape From Treatment; the Different Faces of Leukemic Stem Cells and Therapy Resistance in Acute Myeloid Leukemia. Front Oncol. 2021. 11:659253.
8. Gorrini C, Harris IS, Mak TW. Modulation of oxidative stress as an anticancer strategy. Nat Rev Drug Discov. 2013. 12(12):931-947.
9. Trachootham D, Alexandre J, Huang P. Targeting cancer cells by ROS-mediated mechanisms: a radical therapeutic approach? Nat Rev Drug Discov. 2009. 8(7):579-591.
10. Nizami ZN, Aburawi HE, Semlali A, Muhammad K, Iratni R. Oxidative Stress Inducers in Cancer Therapy: Preclinical and Clinical Evidence. Antioxidants (Basel). 2023. 12(6):1159.
11. Trombetti S, Cesaro E, Catapano R, Sessa R, Lo Bianco A, Izzo P, et al. Oxidative Stress and ROS-Mediated Signaling in Leukemia: Novel Promising Perspectives to Eradicate Chemoresistant Cells in Myeloid Leukemia. Int J Mol Sci. 2021. 22(5):2470.
12. Roder C, Thomson MJ. Auranofin: repurposing an old drug for a golden new age. Drugs R D. 2015. 15(1):13-20.
13. Gamberi T, Chiappetta G, Fiaschi T, Modesti A, Sorbi F, Magherini F. Upgrade of an old drug: Auranofin in innovative cancer therapies to overcome drug resistance and to increase drug effectiveness. Med Res Rev. 2022. 42(3):1111-1146.
14. Pickering IJ, Cheng Q, Rengifo EM, Nehzati S, Dolgova NV, Kroll T, et al. Direct Observation of Methylmercury and Auranofin Binding to Selenocysteine in Thioredoxin Reductase. Inorg Chem. 2020. 59(5):2711-2718.

15. Saei AA, Gullberg H, Sabatier P, Beusch CM, Johansson K, Lundgren B, et al. Comprehensive chemical proteomics for target deconvolution of the redox active drug auranofin. Redox Biol. 2020. 32:101491.
16. Liu N, Li X, Huang H, Zhao C, Liao S, Yang C, et al. Clinically used antirheumatic agent auranofin is a proteasomal deubiquitinase inhibitor and inhibits tumor growth. Oncotarget. 2014. 5(14):5453-5471.
17. Zou P, Chen M, Ji J, Chen W, Chen X, Ying S, et al. Auranofin induces apoptosis by ROS-mediated ER stress and mitochondrial dysfunction and displayed synergistic lethality with piperlongumine in gastric cancer. Oncotarget. 2015. 6(34):36505-36521.
18. Hatem E, El Banna N, Heneman-Masurel A, Baille D, Vernis L, Riquier S, et al. Novel Insights into Redox-Based Mechanisms for Auranofin-Induced Rapid Cancer Cell Death. Cancers (Basel). 2022. 14(19):4864.
19. Kim NH, Park HJ, Oh MK, Kim IS. Antiproliferative effect of gold(I) compound auranofin through inhibition of STAT3 and telomerase activity in MDA-MB 231 human breast cancer cells. BMB Rep. 2013. 46(1):59-64.
20. Nakaya A, Sagawa M, Muto A, Uchida H, Ikeda Y, Kizaki M. The gold compound auranofin induces apoptosis of human multiple myeloma cells through both down-regulation of STAT3 and inhibition of NF-kappaB activity. Leuk Res. 2011. 35(2):243-249.
21. Park SH, Lee JH, Berek JS, Hu MC. Auranofin displays anticancer activity against ovarian cancer cells through FOXO3 activation independent of p53. Int J Oncol. 2014. 45(4):1691-1698.
22. Hatem E, Azzi S, El Banna N, He T, Heneman-Masurel A, Vernis L, et al. Auranofin/Vitamin C: A Novel Drug Combination Targeting Triple-Negative Breast Cancer. J Natl Cancer Inst. 2019. 111(6):597-608.
23. Bottger F, Valles-Marti A, Cahn L, Jimenez CR. High-dose intravenous vitamin C, a promising multi-targeting agent in the treatment of cancer. J Exp Clin Cancer Res. 2021. 40(1):343.
24. El Banna N, Hatem E, Heneman-Masurel A, Leger T, Baille D, Vernis L, et al. Redox modifications of cysteine-containing proteins, cell cycle arrest and translation inhibition: Involvement in vitamin C-induced breast cancer cell death. Redox Biol. 2019. 26:101290.
25. Chen Q, Espey MG, Sun AY, Lee JH, Krishna MC, Shacter E, et al. Ascorbate in pharmacologic concentrations selectively generates ascorbate radical and hydrogen peroxide in extracellular fluid in vivo. Proc Natl Acad Sci U S A. 2007. 104(21):8749-8754.
26. Yun J, Mullarky E, Lu C, Bosch KN, Kavalier A, Rivera K, et al. Vitamin C selectively kills KRAS and BRAF mutant colorectal cancer cells by targeting GAPDH. Science. 2015. 350(6266):1391-1396.
27. Szarka A, Kapuy O, Lorincz T, Banhegyi G. Vitamin C and Cell Death. Antioxid Redox Signal. 2021. 34(11):831-844.
28. Chou TC. Drug combination studies and their synergy quantification using the Chou-Talalay method. Cancer Res. 2010. 70(2):440-446.
29. Podszywalow-Bartnicka P, Kominek A, Wolczyk M, Kolba MD, Swatler J, Piwocka K. Characteristics of live parameters of the HS-5 human bone marrow stromal cell line cocultured with the leukemia cells in hypoxia, for the studies of leukemia-stroma cross-talk. Cytometry A. 2018. 93(9):929-940.

30. Li H, Hu J, Wu S, Wang L, Cao X, Zhang X, et al. Auranofin-mediated inhibition of PI3K/AKT/mTOR axis and anticancer activity in non-small cell lung cancer cells. Oncotarget. 2016. 7(3):3548-3558.
31. Qin S, Wang G, Chen L, Geng H, Zheng Y, Xia C, et al. Pharmacological vitamin C inhibits mTOR signaling and tumor growth by degrading Rictor and inducing HMOX1 expression. PLoS Genet. 2023. 19(2):e1010629.
32. Qin X, Jiang B, Zhang Y. 4E-BP1, a multifactor regulated multifunctional protein. Cell Cycle. 2016. 15(6):781-786.
33. Gajendra S, Gupta R, Thakral D, Gupta SK, Jain G, Bakhshi S, et al. CD34 negative HLA-DR negative acute myeloid leukaemia: A higher association with NPM1 and FLT3-ITD mutations. Int J Lab Hematol. 2023. 45(2):221-228.
34. Webber BA, Cushing MM, Li S. Prognostic significance of flow cytometric immunophenotyping in acute myeloid leukemia. Int J Clin Exp Pathol. 2008. 1(2):124-133.
35. Graczyk-Jarzynka A, Goral A, Muchowicz A, Zagozdzon R, Winiarska M, Bajor M, et al. Inhibition of thioredoxin-dependent H(2)O(2) removal sensitizes malignant B-cells to pharmacological ascorbate. Redox Biol. 2019. 21:101062.
36. Szwed A, Kim E, Jacinto E. Regulation and metabolic functions of mTORC1 and mTORC2. Physiol Rev. 2021. 101(3):1371-1426.
37. Feldman ME, Apsel B, Uotila A, Loewith R, Knight ZA, Ruggero D, et al. Active-site inhibitors of mTOR target rapamycin-resistant outputs of mTORC1 and mTORC2. PLoS Biol. 2009. 7(2):e38.
38. Thoreen CC, Kang SA, Chang JW, Liu Q, Zhang J, Gao Y, et al. An ATP-competitive mammalian target of rapamycin inhibitor reveals rapamycin-resistant functions of mTORC1. J Biol Chem. 2009. 284(12):8023-8032.
39. Gardner TW, Abcouwer SF, Losiewicz MK, Fort PE. Phosphatase control of 4E-BP1 phosphorylation state is central for glycolytic regulation of retinal protein synthesis. Am J Physiol Endocrinol Metab. 2015. 309(6):E546-56.
40. He K, Zheng X, Li M, Zhang L, Yu J. mTOR inhibitors induce apoptosis in colon cancer cells via CHOP-dependent DR5 induction on 4E-BP1 dephosphorylation. Oncogene. 2016. 35(2):148-157.
41. Mraz M, Zent CS, Church AK, Jelinek DF, Wu X, Pospisilova S, et al. Bone marrow stromal cells protect lymphoma B-cells from rituximab-induced apoptosis and targeting integrin alpha-4-beta-1 (VLA-4) with natalizumab can overcome this resistance. Br J Haematol. 2011. 155(1):53-64.
42. Long X, Yu Y, Perlaky L, Man TK, Redell MS. Stromal CYR61 Confers Resistance to Mitoxantrone via Spleen Tyrosine Kinase Activation in Human Acute Myeloid Leukaemia. Br J Haematol. 2015. 170(5):704-18.
43. Capparelli EV, Bricker-Ford R, Rogers MJ, McKerrow JH, Reed SL. Phase I Clinical Trial Results of Auranofin, a Novel Antiparasitic Agent. Antimicrob Agents Chemother. 2017. 61(1):e01947-16.
44. Jiang H, Zuo J, Li B, Chen R, Luo K, Xiang X, et al. Drug-induced oxidative stress in cancer treatments: Angel or devil? Redox Biol. 2023. 63:102754.

FIGURE LEGENDS

FIGURE 1. AUF/VC combinations synergistically killed myeloid leukaemia cells. (A) Six cell lines were treated by AUF, VC and AUF/VC with indicated concentrations for 48 h and stained with PI before proceeding to the cytometric analysis. Results are displayed as PI^- cells/µl. For each set of experiments, the percentage of the surviving fraction was calculated relative to non-treated cells that is set to be 100%. Bar graphs show mean ± SD of at least three independent experiments. Combined drug effects defined by CI are calculated using CompuSyn software and are indicated above histograms. NT, no drug-treated control. (B) Viability of KG1 or K562 leukemia cells co-cultured with stromal HS-5 cells upon AUF 0.5 µM/VC 0.5 mM treatment. The percentage of the surviving cell fraction was calculated and displayed as in (A). The statistical significance was calculated by an unpaired, two tailed *t* test with Welch's correction. ****, $p < 0.0001$.

FIGURE 2. AUF/VC combination rapidly induced ROS elevation and protein oxidation. (A) The KG-1 and K562 cells treated with defined conditions for 2 h were stained with the carboxy-H_2DCFDA and MitoSOX Red sensors before cytometry analysis. A fluorescence distribution histogram, representative of three independent experiments, is presented. X-axis represents fluorescence intensity of DCF or MitoSOX. (B-C) The KG-1 (B) and K562 (C) cells treated with indicated conditions were proceeded for redox western blot analysis for PRDX1 and PRDX3. A representative image of three independent experiments is presented. ox, oxidized form; red, reduced form. Bar graphs (right panels of B and C) show mean ± SD of the quantification of the oxidized form (%) versus total PRDX1 or PRDX3 protein from three independent experiments. NT, no drug-treated control. Ordinary one-way ANOVA (multiple

comparisons) was used to estimate the differences for differently treated cells. *, $p < 0.05$; **, $p < 0.01$; ***, $p < 0.001$; ****, $p < 0.0001$.

FIGURE 3. AUF/VC combination caused rapidly ATP decline and MMP loss in leukaemic cells. (A) ATP levels of KG1 and K562 cells treated by indicated conditions. The ATP levels were evaluated using Promega CellTiter-Glo assay. The ATP level of no drug-treated control (NT) at the defined time point is set as 1. Bar graphs show mean ± SD of at least three independent experiments. The statistical significance between the ATP levels of VC-treated and AUF/VC-treated cells was calculated by an unpaired, two tailed *t* test with Welch's correction. **, $p < 0.01$; ***, $p < 0.001$; ****, $p < 0.0001$. (B) MMP of K562 cells under indicated treatment conditions. Cytometry fluorescence histograms represent the ratio of PE (red)/FITC (green). The percentage of cells showing low MMP is indicated.

FIGURE 4. AUF/VC combination affected mTOR/4E-BP1/p70S6K cell signaling pathway. (A-D). Phosphorylation state of 4E-BP1 (Thr37/46), p70S6K (Thr389) and mTOR (Ser2448) and AKT (Ser473) in response to indicated treatments in KG-1 and K562 cells. For each blot set, the same protein extracts were used for the detection of phosphorylated forms, total proteins and actin as a loading control. Representative blots of three independent protein extracts are presented. Different treatments, indicated by 1 to 8 and applied to A-D, are explained at the bottom of D. Graphs (right panels of A, B, C and D) show the normalized relative quantity of p-4E-BP1, p-p70S6K, p-mTOR and p-AKT, respectively, after treatment with AUF/VC combination for 2 and 4 h, compared with no drug-treated control (NT) set as 1. The statistical significance between the NT and AUF/VC-treated cells was calculated by an unpaired, two tailed *t* test with Welch's correction. *, $p < 0.05$; **, $p < 0.01$; ***, $p < 0.001$; ****, $p < 0.0001$. (E) Effect of MHY1485 on AUF/VC-induced 4E-BP1 dephosphorylation. Bar graph shows

mean ± SD of the normalized relative quantity of p-4E-BP1 under indicated conditions from three independent experiments, with no drug-treated control cells (NT) set as 1. Ordinary one-way ANOVA (multiple comparisons) was used to estimate the differences between differently treated cells. ns, not significant; **, $p < 0.01$; ****, $p < 0.0001$.

FIGURE 5. Global nascent protein translation measurement using O-Propargyl-puromycin-based Protein Synthesis Assay Kit. Nascent polypeptide synthesis was detected with a Cytoflex flow cytometer using the FITC channel. Negative control corresponds to cells without drug treatments and without processing protein synthesis assay while positive control corresponds to cells without drug treatment but tested with protein synthesis assay. Cells treated with cycloheximide were used as a control for protein synthesis inhibition. Representative histograms of three independent sets of experiments are presented. Fluorescence intensity (geometric mean) was measured by Kaluza software. Graphs (right panels) show the relative inhibition of protein synthesis (mean ± SD of three independent experiments) compared with positive control cells (set as 100%). The statistical significance was calculated by an unpaired, two tailed *t* test with Welch's correction.

FIGURE 6. The effect of AUF, VC and AUF/VC combination on haematopoietic $CD34^+$ cells from AML samples and normal cord blood (CB). **(**A) Example of flow cytometry analysis with AML_07. The live $CD34^+$ population ($CD34^+$ Sytox $Blue^-$) was gated and indicated (black circle). (B) Viable $CD34^+$ cells ($CD34^+$ Sytox $Blue^-$) of individual AML samples following indicated treatments relative to no drug-treated control. Data of 19 AML samples (AML_5, 19 and AML_04 excluded) are presented. The graphs depict mean ± SD, and each dot corresponds to an individual sample. Three combinations, AUF 0.25 µM/VC 0.25 mM, AUF 0.5 µM/VC 0.5 mM and AUF 1 µM/VC 1 mM, are represented by Combination 1, Combination 2 and

Combination 3, respectively. NT, no drug-treated control. (C) Western blot analysis of the phosphorylation state of 4E-BP1 (Thr37/46) in $CD34^+$-enriched primary leukaemia cells from AML_6 and AML_16 in response to indicated treatments for 4 h. For each blot set, the same protein extracts were used for the detection of phosphorylated forms, total proteins and actin as a loading control. (D) Viable $CD34^+$ cells ($CD34^+$ Sytox $Blue^-$) of 5 individual CB samples following indicated treatments relative to no drug-treated control. The graphs depict mean ± SD, and each dot corresponds to an individual sample. Indications for treatment conditions are as B. (E) Comparison of survival of AML $CD34^+$ cells (n = 19, as in B) and CB $CD34^+$ cells (n = 5, as in D) in response to treatments of AUF, VC and their combinations. The graphs depict mean ± SD, and each dot corresponds to an individual sample. In each group, the statistical significance was calculated by an unpaired, two tailed *t* test with Welch's correction. Combination 1, Combination 2 and Combination 3 are as in B.

FIGURE 7. The effect of AUF, VC and AUF/VC combination on colony-forming ability of AML and cord blood samples. (A) The *in vitro* colony-forming ability of five AML samples were analyzed under indicated treatments. For each sample, the mean number of colony-forming unit (CFU) from triplicate dishes was calculated and the percentage is relative to the no drug-treated control (set to be 100%). Representative images with low magnification from AML_2 and AML_6 samples are shown. (B) A summary of colony-forming ability of 4 cord blood samples under indicated treatments. For each sample, the mean number of CFU from triplicate dishes was calculated and the percentage is relative to no drug-treated control (set to be 100%). Bar graphs show mean ± SD. Representative CFU images with low magnification are shown. NT, no drug-treated control.

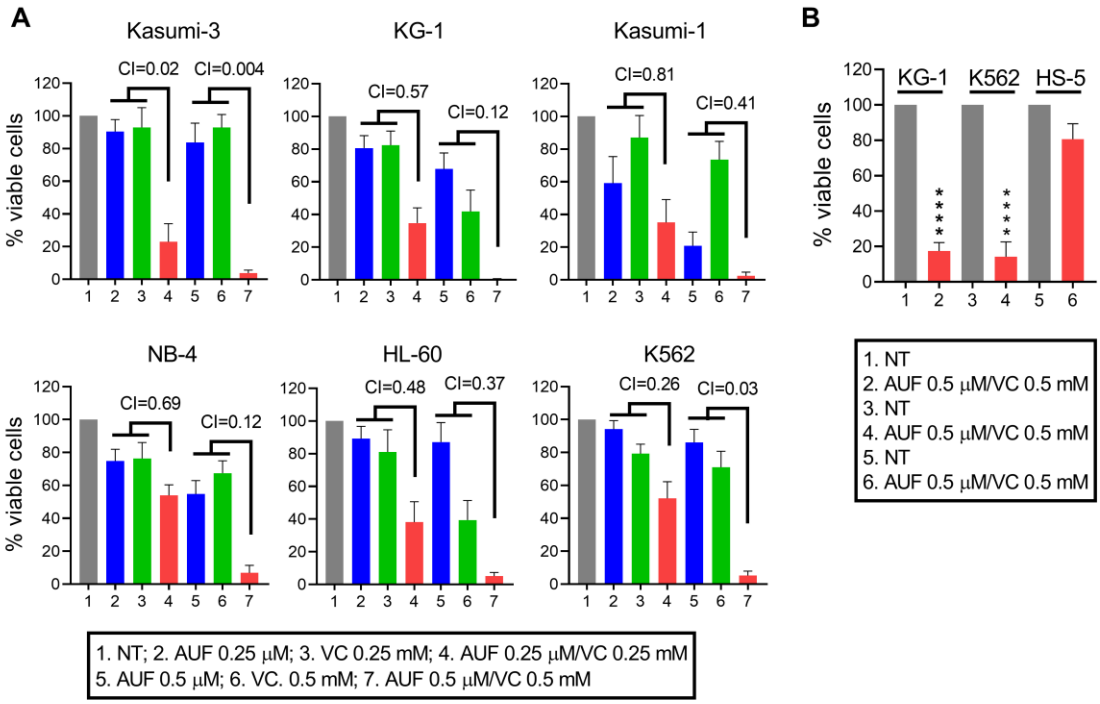
A
Kasumi-3
CI=0.02
CI=0.004
KG-1
CI=0.57
CI=0.12
Kasumi-1
CI=0.81
CI=0.41
NB-4
CI=0.69
CI=0.12
HL-60
CI=0.48
CI=0.37
K562
CI=0.26
CI=0.03
% viable cells
1. NT; 2. AUF 0.25 μM; 3. VC 0.25 mM; 4. AUF 0.25 μM/VC 0.25 mM
5. AUF 0.5 μM; 6. VC. 0.5 mM; 7. AUF 0.5 μM/VC 0.5 mM
B
KG-1
K562
HS-5
****
****
% viable cells
1. NT
2. AUF 0.5 μM/VC 0.5 mM
3. NT
4. AUF 0.5 μM/VC 0.5 mM
5. NT
6. AUF 0.5 μM/VC 0.5 mM

Figure 1

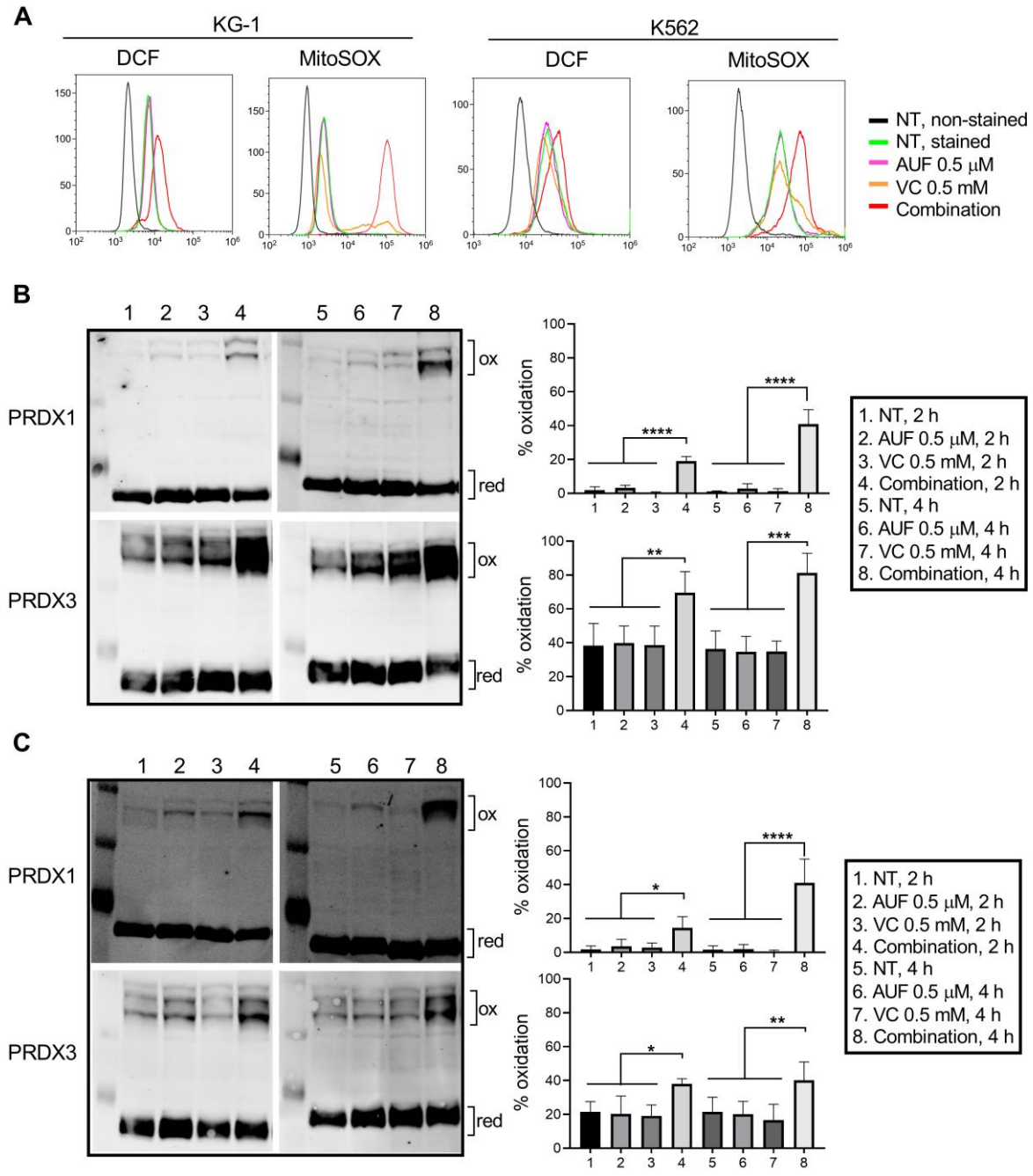
A
KG-1
K562
DCF
MitoSOX
DCF
MitoSOX
NT, non-stained
NT, stained
AUF 0.5 μM
VC 0.5 mM
Combination
B
1 2 3 4 5 6 7 8
PRDX1
PRDX3
ox
red
% oxidation
1. NT, 2 h
2. AUF 0.5 μM, 2 h
3. VC 0.5 mM, 2 h
4. Combination, 2 h
5. NT, 4 h
6. AUF 0.5 μM, 4 h
7. VC 0.5 mM, 4 h
8. Combination, 4 h
C
1 2 3 4 5 6 7 8
PRDX1
PRDX3
ox
red
% oxidation
1. NT, 2 h
2. AUF 0.5 μM, 2 h
3. VC 0.5 mM, 2 h
4. Combination, 2 h
5. NT, 4 h
6. AUF 0.5 μM, 4 h
7. VC 0.5 mM, 4 h
8. Combination, 4 h

Figure 2

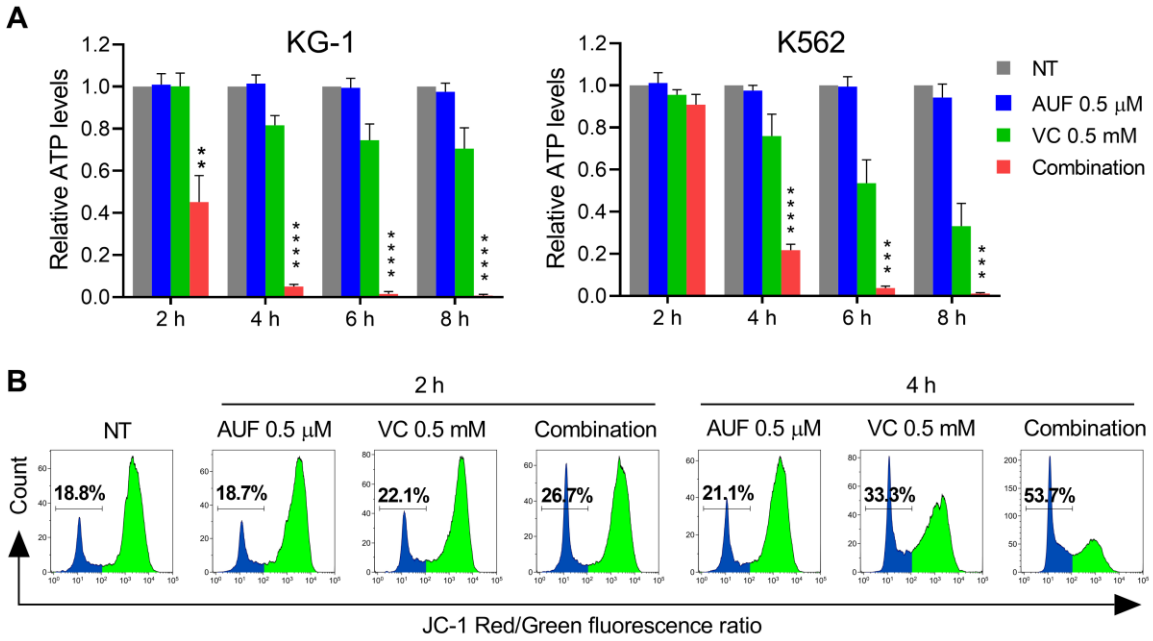
A
KG-1
K562
Relative ATP levels
1.2
1.0
0.8
0.6
0.4
0.2
0.0
2 h
4 h
6 h
8 h
NT
AUF 0.5 μM
VC 0.5 mM
Combination
B
2 h
4 h
NT
AUF 0.5 μM
VC 0.5 mM
Combination
AUF 0.5 μM
VC 0.5 mM
Combination
Count
18.8%
18.7%
22.1%
26.7%
21.1%
33.3%
53.7%
JC-1 Red/Green fluorescence ratio

Figure 3

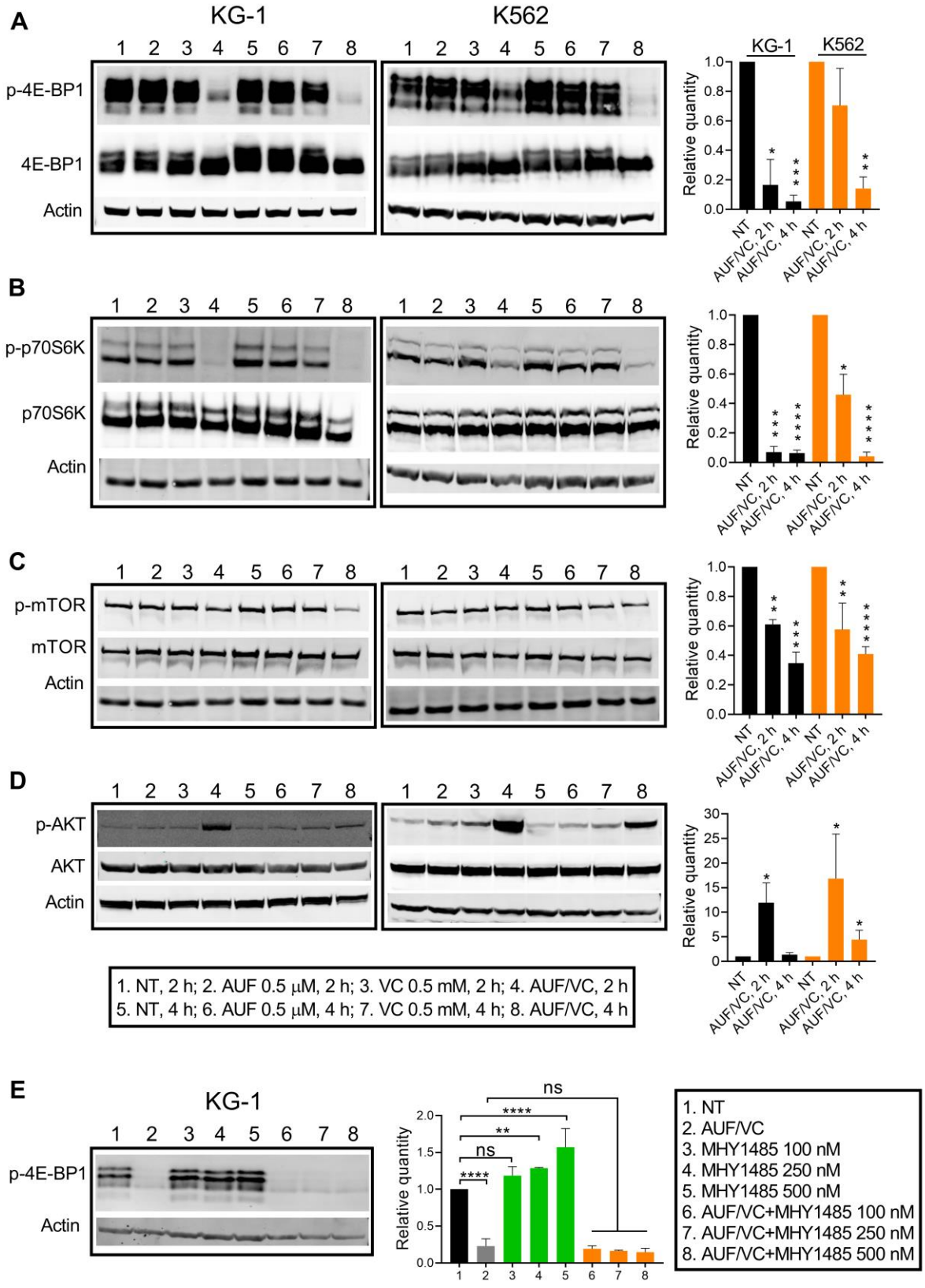
A
KG-1
K562
1 2 3 4 5 6 7 8
p-4E-BP1
4E-BP1
Actin
Relative quantity
NT
AUF/VC, 2 h
AUF/VC, 4 h
B
p-p70S6K
p70S6K
Actin
C
p-mTOR
mTOR
Actin
D
p-AKT
AKT
Actin
1. NT, 2 h; 2. AUF 0.5 μM, 2 h; 3. VC 0.5 mM, 2 h; 4. AUF/VC, 2 h
5. NT, 4 h; 6. AUF 0.5 μM, 4 h; 7. VC 0.5 mM, 4 h; 8. AUF/VC, 4 h
E
KG-1
p-4E-BP1
Actin
ns
1. NT
2. AUF/VC
3. MHY1485 100 nM
4. MHY1485 250 nM
5. MHY1485 500 nM
6. AUF/VC+MHY1485 100 nM
7. AUF/VC+MHY1485 250 nM
8. AUF/VC+MHY1485 500 nM

Figure 4

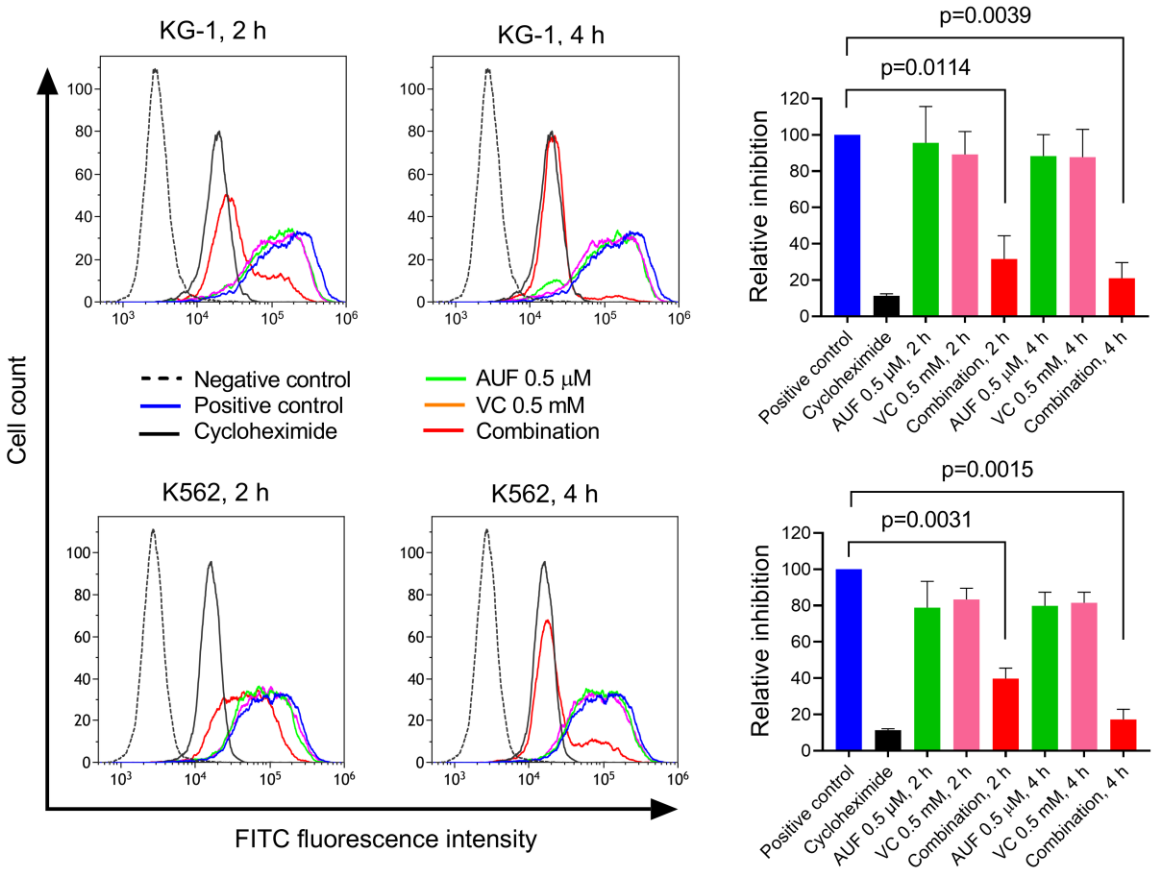
KG-1, 2 h
KG-1, 4 h
K562, 2 h
K562, 4 h
Cell count
FITC fluorescence intensity
Negative control
Positive control
Cycloheximide
AUF 0.5 μM
VC 0.5 mM
Combination
p=0.0039
p=0.0114
Relative inhibition
Positive control
Cycloheximide
AUF 0.5 μM, 2 h
VC 0.5 mM, 2 h
Combination, 2 h
AUF 0.5 μM, 4 h
VC 0.5 mM, 4 h
Combination, 4 h
p=0.0015
p=0.0031

Figure 5

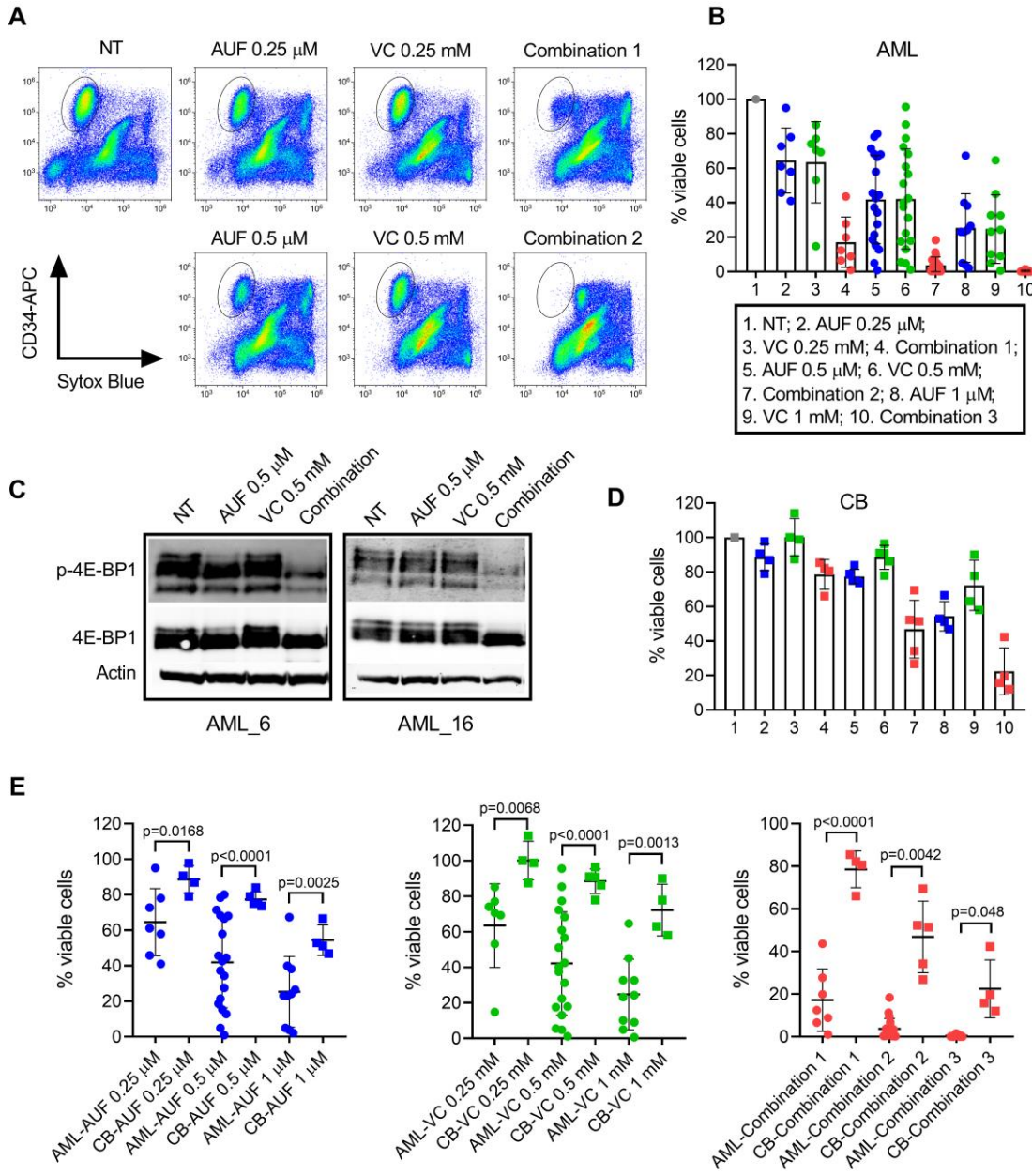
A
NT
AUF 0.25 μM
VC 0.25 mM
Combination 1
AUF 0.5 μM
VC 0.5 mM
Combination 2
CD34-APC
Sytox Blue
B
AML
% viable cells
1. NT; 2. AUF 0.25 μM;
3. VC 0.25 mM; 4. Combination 1;
5. AUF 0.5 μM; 6. VC 0.5 mM;
7. Combination 2; 8. AUF 1 μM;
9. VC 1 mM; 10. Combination 3
C
NT
AUF 0.5 μM
VC 0.5 mM
Combination
p-4E-BP1
4E-BP1
Actin
AML_6
AML_16
D
CB
% viable cells
E
% viable cells
p=0.0168
p<0.0001
p=0.0025
AML-AUF 0.25 μM
CB-AUF 0.25 μM
AML-AUF 0.5 μM
CB-AUF 0.5 μM
AML-AUF 1 μM
CB-AUF 1 μM
p=0.0068
p<0.0001
p=0.0013
AML-VC 0.25 mM
CB-VC 0.25 mM
AML-VC 0.5 mM
CB-VC 0.5 mM
AML-VC 1 mM
CB-VC 1 mM
p<0.0001
p=0.0042
p=0.048
AML-Combination 1
CB-Combination 1
AML-Combination 2
CB-Combination 2
AML-Combination 3
CB-Combination 3

Figure 6

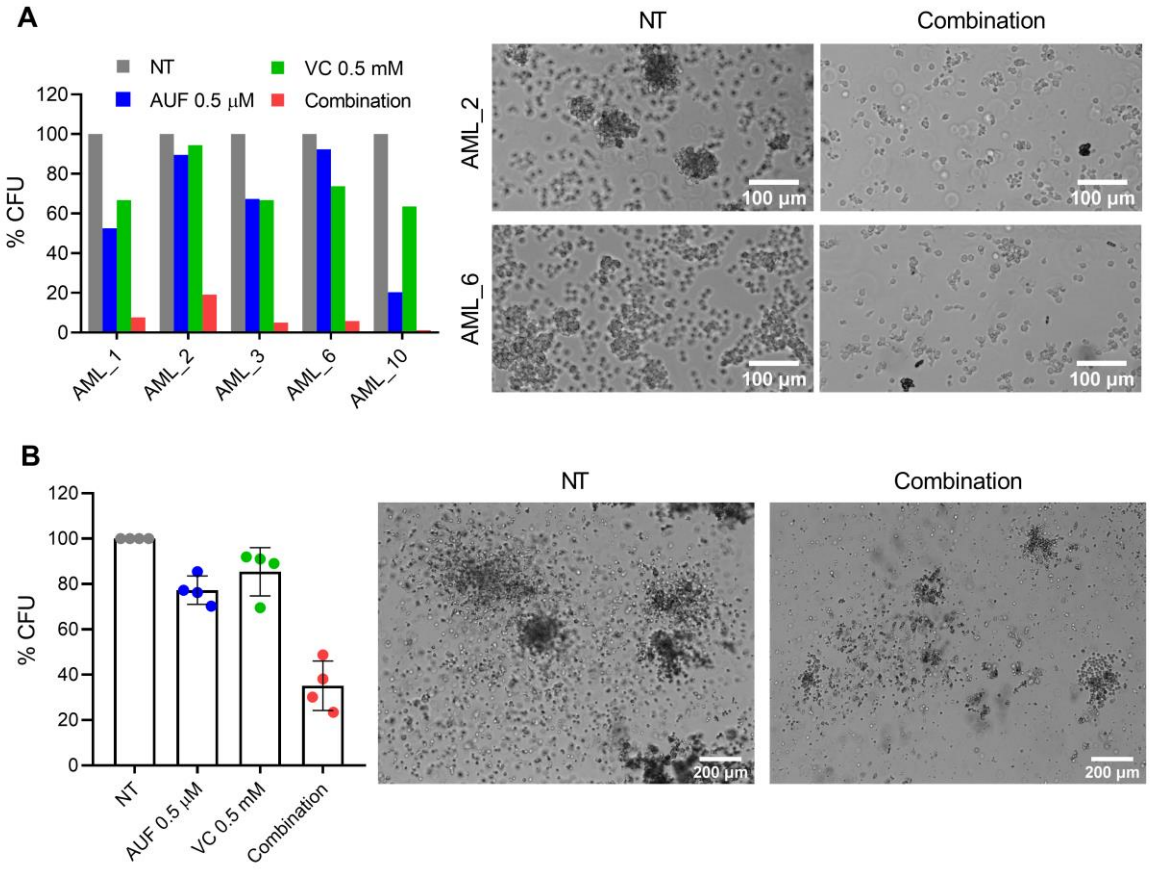
A
NT
VC 0.5 mM
AUF 0.5 μM
Combination
% CFU
120
100
80
60
40
20
0
AML_1
AML_2
AML_3
AML_6
AML_10
NT
Combination
AML_2
AML_6
100 μm
B
% CFU
NT
AUF 0.5 μM
VC 0.5 mM
Combination
200 μm

Figure 7

SUPPLEMENTARY INFORMATION

Targeting the redox vulnerability of acute myeloid leukaemia cells with a combination of auranofin and vitamin C

Zhiliang Hei, Shujun Yang, Guifang Ouyang, Jolimar Hanna, Michel Lepoivre, Tony Huynh, Lorea Aguinaga, Bruno Cassinat, Nabih Maslah, Mickaël Bourge, Marie-Pierre Golinelli-Cohen, Olivier Guittet, Cindy Vallières, Laurence Vernis, Pierre Fenaux*, Meng-Er Huang*

* Corresponding authors

Pierre Fenaux, pierre.fenaux@aphp.fr

Meng-Er Huang, meng-er.huang@cnrs.fr

Supplementary Materials and Methods

Supplementary Table S1. Clinical characteristics of AML samples used in this study.

Supplementary Figure S1. ATP levels of Kasumi-3 and HL-60 cells treated by indicated conditions.

Supplementary Figure S2. Phorsphorylation state of 4E-BP1 (Thr37/46) in Kasumi-3 and HL-60 cells in response to indicated treatments.

Supplementary Figure S3. Gating strategy for identification and enumeration of total live $CD34^+$ cells ($CD34^+$ Sytox $Blue^–$).

Supplementary Figure S4. The effect of AUF, VC and AUF/VC combination on AML_04 sample, measured by flow cytometry.

SUPPLEMENTARY MATERIALS AND METHODS

Cell lines and reagents

Kasumi-3 (AML, FAB M0), Kasumi-1 (AML, FAB M2) were purchased from Leibniz Institute DSMZ-German Collection of Microorganisms and Cell Cultures GmbH (Braunschweig, Germany), HL-60 (AML) and HS-5 cells from American Type Culture Collection (Manassas, VA). KG-1 (AML), K562 (chronic myeloid leukaemia at blast crisis) and NB-4 (AML, FAB M3) were kindly provided by Dr Christine Chomienne (Saint-Louis Hospital, Paris). All cells were maintained in RPMI 1640 medium supplemented with 10% fetal bovine serum (FBS), 2 mM L-glutamate, and 100 units of penicillin/streptomycin at 37 °C with 5% CO_2. All cell lines were authenticated at the beginning of the present study using standard DNA microsatellite short tandem repeat method. Morphology of cell lines was monitored routinely, and cell lines were routinely subjected to mycoplasma detection using a mycoplasma detection kit (LT07-218, Lonza).

AUF was purchased from Enzo Life Sciences. L-ascorbic acid (vitamin C, VC), N-ethylmaleimide (NEM), dimethyl sulfoxide (DMSO), dithiothreitol (DTT), trichloroacetic acid, Ficoll-Paque Plus were purchased from Merck/Sigma-Aldrich. Propidium iodide (PI), eFluor450, CFSE, 6-carboxy-2',7'-dichlorodihydrofluorescein diacetate (carboxy-H_2DCFDA), MitoSOX Red and Sytox Blue were from Thermo Fisher Scientific. MHY1485 was from Selleckchem. Antibodies anti-PRDX3 (#ab16751) and anti-ß-actin (#sc-1616) were from Abcam and Santa Cruz Biotechnology, respectively. All following antibodies were from Cell Signaling Technology: PRDX1 (#8499), phospho-Akt (Ser473) (#4060), Akt (9272), phospho-p70S6K (Thr389) (#9205), p70S6K (#2708), phospho-mTOR (Ser2448) (#2971), mTOR (#2972), phospho-4E-BP1 (Thr37/46) (#2855), 4E-BP1 (#9644). Allophycocyanin (APC) anti-human CD34 antibody (#343510) and phycoerythrin (PE) anti-human CD38 antibody (#356603) were from BioLegend. Brilliant stain buffer plus (#566385) was from BD

Biosciences. CD34 MicroBead kit (#130-046-702) was from Miltenyi Biotec. Recombinant human haematopoietic growth factors were from PEPROTECH: SCF (#300-07), G-CSF (#300-23), GM-CSF (#300-03), Flt3-Ligand (#300-19), TPO (#300-18), IL-3 (#200-03) and IL-6 (#200-06).

Cell death assessment for cells from cell lines

Cells were seeded in 6-well plates at a density of 2×10^5 cells per ml for overnight incubation and subjected to treatments for 48 h. Cells were then harvested, and washed in PBS containing 1% fetal bovine serum (FBS) and resuspended in an equal volume of PBS containing 1% FBS and PI (1 µg/ml) before being analyzed by a Cytoflex S flow cytometer (Beckman Coulter). At least 10 000 events were acquired for each sample for analysis using CytExpert software (Beckman Coulter). Detection of PI fluorescence was evaluated by 561-nm laser excitation with emission detection through a 610/20-nm bandpass filter. Cells were firstly identified by a "Cells" gate in FSC (Forward scatter)/SSC (Side Scatter) dot plot, and then further gated by their side scatter-height (SSC-H) and side scatter-area (SSC-A) to select single cells (Singlets), Absolute PI^- cell counts inside "Singlets" gate after different treatments were calculated, displayed as PI^- cells/µl, and normalized to the cell counts in the no drug-treated control (set to be 100%). Data of combined drug effects were analyzed by the Chou-Talalay method using CompuSyn software.[1] Drug synergistic, additive, and antagonistic effects are defined by combination index (CI) values of < 0.9, 0.9–1.1, and > 1.1, respectively.

HS-5 and KG-1 co-culture, HS-5 and K562 co-culture and cytometer-based analysis followed the experimental setup described by Podszywalow-Bartnicka *et al*.[2] HS-5 cells were labeled with 10 µM eFluor450, and KG-1 or K562 cells were labeled with 2.5 µM CFSE according to the manufacturer's protocols. After labeling and washing, leukemia cells were seeded at 1:1 leukemia-to-stroma ratio, in 12-well plates at a density of 2×10^5 cells per ml in

RPMI 1640 medium. After 24 h incubation, cells were treated with AUF/VC combinations for 48 h. Cells were then harvested, and washed in PBS containing 1% FBS and resuspended in an equal volume of PBS containing 1% FBS and PI (1 μg/ml) before being analyzed by a Cytoflex S flow cytometer. For cell-type separation, cells were gated on the basis of the fluorescence of eFluor450 (excited by a 488-nm laser and emission collected through a 450/45-nm bandpass filter) or CFSE (excited by a 488-nm laser and emission collected through a 525/40-nm bandpass filter). Viable and dead cells in each population was discriminated by PI fluorescence. Density of viable cells was displayed as PI^- cells/μl, and normalized to the cell counts in the no drug-treated control (set to be 100%).

Oxidative stress assessment

Cells were seeded in 6-well plates at a density of 2×10^5 cells per ml and were subjected to different treatments on the next day. Cells were then washed with 37°C PBS and incubated in 1 mL of DMEM without phenol red (Thermo Fisher Scientific) containing 10 μM carboxy-H_2DCFDA or 5 μM of MitoSOX Red. After incubation for 30 min at 37°C in a 5% CO_2 atmosphere, cells were collected, washed and resuspended in PBS containing 1% FBS. The fluorescence yielded from the staining reagents was detected using a Cytoflex S flow cytometer: carboxy-H_2DCFDA was excited by a 488-nm laser and emission was collected through a 525/40-nm bandpass filter; MitoSOX was excited by a 561-nm laser and emission was collected through a 585/42-nm bandpass filter. At least 10 000 events were acquired for each sample. Results were analyzed and displayed using Kaluza software (Beckman Coulter). For the detection of reduced and oxidized peroxiredoxin 1 (PRDX1) and peroxiredoxin 3 (PRDX3), cells were seeded in 100-mm cell culture dishes at a density of 2×10^5 cells per ml overnight before subjecting them to defined treatments. Redox western blots were processed as described below.

Intracellular ATP content analysis and mitochondrial membrane potential (MMP) measurement

The CellTiter-Glo Luminescent Cell Viability Assay Kit (Promega) was used to determine intracellular ATP content. Cells were incubated and treated like for PI-based cell death assay in 6-well plates and aliquots were removed at defined times for ATP quantification according to the manufacturer's protocols. The chemiluminescence intensity was measured by a SpectraMax M3 MultiMode microplate reader (Molecular Devices)**.** Each point in one experiment was run in triplicate and each condition was repeated by at least three independent experiments. Relative ATP levels were expressed compared to that of no drug-treated control cells (set to be 100%). JC-1 was used to evaluate changes in MMP. JC-1 enters the mitochondria and changes its fluorescent properties based on the aggregation of the probe. In healthy cells with high MMP, JC-1 forms complexes known as J-aggregates with intense red fluorescence. In cells with low MMP, JC-1 remains in the monomeric form, which exhibits green fluorescence. The ratio of red to green fluorescence reflects the polarization of the mitochondrial membrane. Cells incubated and treated like for PI-based cell death assay in 6-well plates were collected and washed in PBS. The samples were then incubated in serum- and phenol red-free DMEM for 20 min at 37 °C in the dark in the presence of JC-1 (1 μg/ml) before being rinsed with PBS and immediately analyzed using Cytoflex S flow cytometer at excitation wavelengths of 488 nm and 561 nm. Emission data were collected through 525/40-nm bandpass filter (FITC) for green fluorescence and 585/42-nm bandpass filter (PE) for red fluorescence. The red (PE)-to-green (FITC) fluorescence ratio was employed to evaluate the changes in MMP.

Western blotting and redox western blotting

Cells were seeded in 6-well plates at a density of 2×10^5 cells per ml and were subjected to different treatments on the next day. Classical western blots and redox western blots were

processed as described previously.[3] Briefly, for classic western blotting, cells were lysed in M-PER protein extraction reagent (Pierce) supplemented with 0.5 mM DTT, complete protease inhibitor cocktail (Roche Diagnostics) and phosphatase inhibitor cocktail (Roche Diagnostics). Lysates were resolved by 7% (for mTOR detection) or 12% NuPAGE Bis-Tris gel (for other proteins) with MOPS buffer (Invitrogen) under reducing conditions. For PRDX1 and PRDX3 redox western blotting, cells in culture were acid-quenched with ice-cold 10% TCA, harvested, washed with acetone and dissolved in lysis buffer (100 mM Tris-Cl, 1% SDS, 10 mM EDTA, pH 8.8) supplemented with 50 mM NEM. Following overnight incubation under shaking at 30 °C, insoluble proteins were removed by centrifugation. Each sample containing about 30 μg of proteins was separated by 12% Bis-Tris gel with MOPS buffer under non-reducing condition. For both classic and redox western blotting, blots after incubation with first antibodies were washed and probed with IRDye 680- or IRDye 800cw-conjugated secondary antibody (LI-COR Biosciences) and then analyzed using an Odyssey Infrared Imaging System (LI-COR). Scanned images and band integrated intensity were analyzed and quantified by Odyssey v3.0 software.

Global nascent protein translation measurement

Protein Synthesis Assay Kit (#ab239725, Abcam) based on O-Propargyl-puromycin (OP-puro) was used for the detection of global nascent proteins of leukaemia cells following the instructions of the manufacturer. Cycloheximide was used as a positive control for protein translation inhibition. Briefly, cells were seeded in 6-well plates at a density of 2×10^5 cells per ml and were subjected to different treatments for different times on the next day. Cells were collected after replacement of fresh medium with protein label for 2 h. After fixation and permeabilization, the reaction cocktail was added and incubated with the cells for 30 min. Nascent polypeptides synthesis was detected with a Cytoflex S flow cytometer at FITC channel

with an excitation wavelength of 488 nm and emission collected through a 525/40-nm bandpass filter. Results were analyzed and displayed using Kaluza software.

Primary AML samples and normal haematopoietic specimens

Peripheral blood samples or bone marrow samples from 22 AML patients were used in this study. The clinical data of these patients are detailed in Table S1. Both AML samples and umbilical cord blood cells from Saint-Louis Hospital (Paris, France) were obtained from donors after informed consent and in compliance with the Declaration of Helsinki. The study involving AML samples from the Department of Hematology of The First Affiliated Hospital of Ningbo University (Ningbo, China) were obtained after informed consent, and the study was approved by the Ethics Committee of The First Affiliated Hospital of Ningbo University and was in accordance with the Declaration of Helsinki.

Blood or bone marrow samples were subjected to Ficoll-Paque Plus density gradient separation to isolate mononuclear cells. In some cases at this stage, mononuclear cells were cryopreserved in freezing medium consisting of 90% FBS and 10% DMSO. The viability of the leukemic cells after thawing was 60% to 85%. Fresh or thawed cells were then plated at 2 $\times 10^5$ cells/ml in RPMI 1640, 10% FBS, 2 mM L-glutamine, supplemented with 50 ng/ml SCF, 50 ng/ml Flt3-Ligand, 10 ng/ml G-CSF, 10 ng/ml GM-CSF, 10 ng/ml IL-3, 10 ng/ml IL-6, 15 ng/ml TPO. Cells were cultured in the above medium at 37°C in a humidified atmosphere containing 5% CO_2 for at least 6 h before the addition of drugs. After drug treatment for 48 h or 72 h, cells were harvested, washed with PBS, and resuspended in 100 µL of PBS/1% FBS containing 1X brilliant stain buffer plus. The cells were then incubated in the presence or absence of CD34-APC and CD38-PE antibodies in the dark at room temperature for 30 min. Once washed with PBS, the cells were resuspended in an equal volume of PBS containing 1% FBS and 1 µM Sytox Blue and analyzed by a Cytoflex S flow cytometer (Sytox Blue, PE and

APC were respectively excited at 405, 561 and 638 nm, and emission was respectively collected through 450/45-, 585/42- and 660/20- nm bandpass filter) or a FACSCanto flow cytometer (Becton Dickinson, Sytox Blue, PE and APC were respectively excited at 405, 488 and 640 nm, and emission was respectively collected through 450/50-, 585/15- and 660/20- nm bandpass filter). For each sample, the maximum number of events were collected. Sytox Blue staining was used to discriminate dead cells. Live $CD34^+$ cells ($CD34^+$ Sytox $Blue^-$) were gated and scored. Results were analyzed and displayed using Kaluza software.

Two AML samples were used for western blot analysis of the phosphorylation/dephosphorylation of 4E-BP1. Cryopreserved mononuclear cells were thawed and recovered and $CD34^+$ cells were purified by positive selection using the midi MACS immunomagnetic separation system (Miltenyi Biotec) according to the manufacturer's instructions. Purified CD34+ cells were seeded at 2×10^5 cells/ml in RPMI 1640, 10% FBS, 2 mM L-glutamine, supplemented with growth factors described above and cultured for 24 h before the addition of drugs. Because of limited $CD34^+$ cells, only 4 h-treatment was applied. Classic western blot was performed as described above.

Methylcellulose colony-forming assay

Mononuclear cells isolated from AML or cord blood sample were first precultivated for at least 6 h in RPMI 1640 medium containing various growth factors as above. A desired number of cells was removed and resuspended in 2% FBS/IMDM medium (20X of the final cell number needed for a given experiment). An appropriate volume of cells was transferred to the MethoCult GF H4034 Optimum methylcellulose-based medium (#04034, Stemcell Technologies) to a final density of 2×10^5 cells/ml. This medium supports optimal growth of granulocyte-macrophage progenitor cells (CFU-GM, CFU-G and CFU-M), erythroid progenitor cells (BFU-E and CFU-E), and multipotential granulocyte, erythroid, macrophage,

megakaryocyte progenitor cells (CFU-GEMM). AUF, VC or AUF/VC at appropriate concentrations (20X of the final concentration) was added onto the cells directly within the methylcellulose medium. After vigorously vortexing, 1.1 ml of cell mixture was transferred to a 35-mm culture dish and then incubated at 37°C in a humidified atmosphere at 5% CO_2 for 12–14 days. Each treatment point was prepared in triplicates. Colonies were scored microscopically with an inverted microscope. Representative CFU images were taken with a DMI6000 widefield microscope (Leica) using the 5× or 10× objective.

1. Chou TC. Drug combination studies and their synergy quantification using the Chou-Talalay method. Cancer Res. 2010. 70(2):440-446.
2. Podszywalow-Bartnicka P, Kominek A, Wolczyk M, Kolba MD, Swatler J, Piwocka K. Characteristics of live parameters of the HS-5 human bone marrow stromal cell line cocultured with the leukemia cells in hypoxia, for the studies of leukemia-stroma cross-talk. Cytometry A. 2018. 93(9):929-940.
3. He T, Hatem E, Vernis L, Lei M, Huang ME. PRX1 knockdown potentiates vitamin K3 toxicity in cancer cells: a potential new therapeutic perspective for an old drug. J Exp Clin Cancer Res. 2015. 34:152.

SUPPLEMENTARY TABLE S1.

Supplementary Table S1. Clinical characteristics of AML samples used in this study						
Patient	**Sample ID**	**FAB subtype**	**Cytogenetics**	**Mutations**	**ELN 2022 Risk group**	**Previous therapy**
1	AML_01	M1	Normal	NPM1, FLT3-ITD, BCOR, ASXL1, SF3B1, CTCF	Intermediate	No
2	AML_02	M5b	t(6;11)	None	Adverse	Azacitidine and Venetoclax
3	AML_03	NA	del(20q)	CALR, NFE2, ASXL1	Adverse	Azacitidine and Venetoclax
4	AML_04	M5	tri(8) tri(15)	TET2, BRAF	Intermediate	Hydroxyurea
5	AML_05	M2	del(20q)	NPM1, FLT3-ITD, TET2, DNMT3A	Favorable	Hydroxyurea
6	AML_06	M4	Normal	NPM1, IDH1, FLT3-TKD, DNMT3A, PRPF8	Favorable	No
7	AML_07	NA	ND	ND	NA	No
8	AML_08	M4	Normal	NPM1, FLT3-ITD, ETV6, DNMT3A	Favorable	Hydroxyurea
9	AML_09	NA	Normal	U2AF1, NF1	Adverse	Azacitidine
10	AML_10	NA	Normal	SF3B1, STAG2, SRSF2	Adverse	Azacitidine
11	AML_11	NA	Complex and monosomal	BCOR, U2AF1, CUX1	Adverse	No
12	AML_12	NA	Complex and monosomal	TP53	Adverse	No
13	AML_13	NA	Normal	IDH1, SRSF2, STAG2, CEBPA, DNMT3A	Adverse	No
14	AML_14	M1	tri(11)	IDH1, SRSF2, ASXL1, RUNX1	Adverse	No
15	AML_15	NA	Complex and monosomal	TET2, SRSF2, SETD1B, EP300, JAK2, SETBP1	Adverse	No
16	AML_16	NA	Normal	biallelic CEBPA, GATA2, RAD21, NRAS	Favorable	No
17	AML_17	M4	47, XX,+8[20]	RUNX1, ASXL1, SETBP1, PHF6	NA	No
18	AML_18	M0	Normal	BCOR, RUNX1, TP53, BCORL1, ETV6, TET2	NA	No
19	AML_19	M5	Normal	CEBPA, CSF3R, NRAS, ATM	NA	No
20	AML_20	M4	46,XX,t(8;21)(q22;q22),t(11;15)(q23;q11)[7]/46,XX[13]	AML1-ETO+	NA	No
21	AML_21	M4	46,XY,t(8;21)(q22;q22)[11]/45,X,-Y,idem[9]	FLT3, RAD21, AML1-ETO+	NA	No
22	AML_22	M5	ND	KIT, WT1, PTPN11	NA	No

NA, not available; ND, not determined; AML_1-16 were peripheral blood samples and AML_17-22 were bone marrow samples.

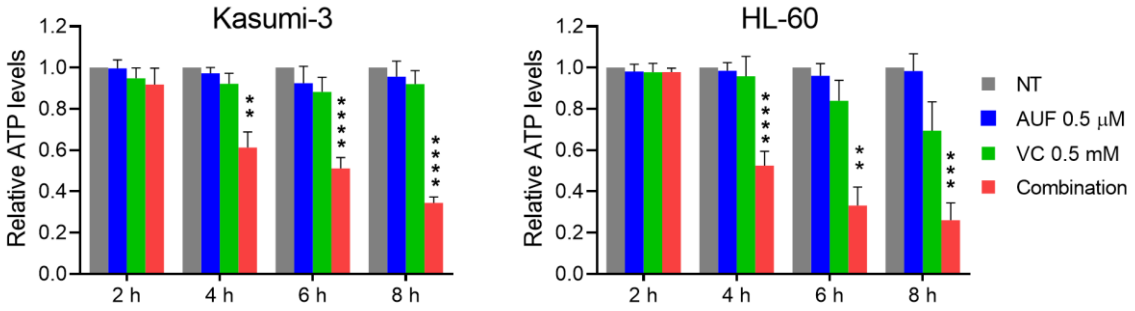

SUPPLEMENTARY FIGURE S1. ATP levels of Kasumi-3 and HL-60 cells treated by indicated conditions. The ATP levels were evaluated using Promega CellTiter-Glo assay and that of no drug-treated control (NT) at the defined time point is set as 1. Bar graphs show mean ± SD of at least three independent experiments. The statistical significance between the ATP levels of VC-treated and AUF/VC-treated cells was calculated by an unpaired, two tailed *t* test with Welch's correction. **, $p < 0.01$; ***, $p < 0.001$; ****, $p < 0.0001$.

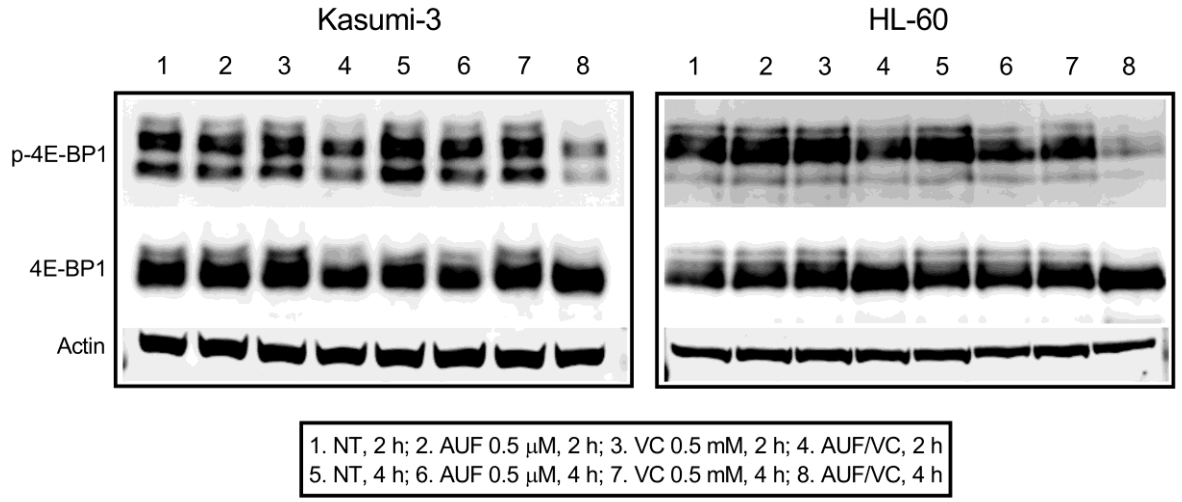

SUPPLEMENTARY FIGURE S2. Phorsphorylation state of 4E-BP1 (Thr37/46) in Kasumi-3 and HL-60 cells in response to indicated treatments. For each panel, the same protein extracts were used for detection of the phosphorylated form, corresponding total protein, and actin as a loading control. Representative blots from two independent experiments (protein extracts) are presented. NT, no drug-treated control.

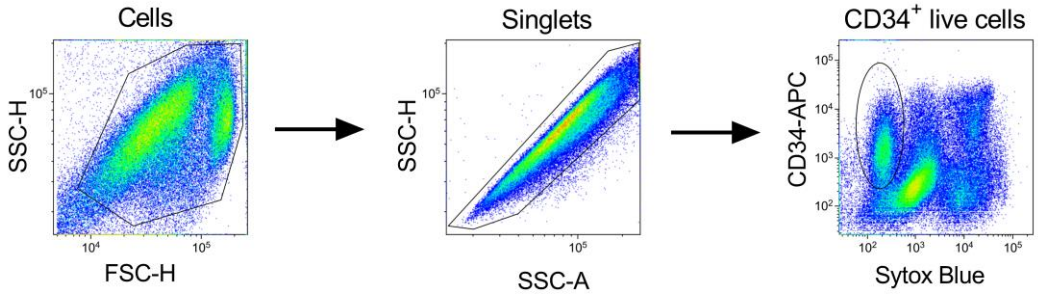

SUPPLEMENTARY FIGURE S3. Gating strategy for identification and enumeration of total live CD34$^+$ cells (CD34$^+$ Sytox Blue$^-$). Forward scatter (FSC) vs side scatter (SSC) density plot profile distinguished intact cells from cellular debris. The selected gate (Cells) was further gated by its side scatter-height (SSC-H) and side scatter-area (SSC-A) to select single cells (Singlets), from which the live CD34$^+$ population (CD34$^+$ Sytox Blue$^-$) containing live stem and progenitor cells and blasts was gated (black circle). Absolute cell counts inside the gates were calculated and normalized to the cell counts in the no drug-treated control (represented as percentage). Patient sample experiments were usually performed once due to limited available cell number.

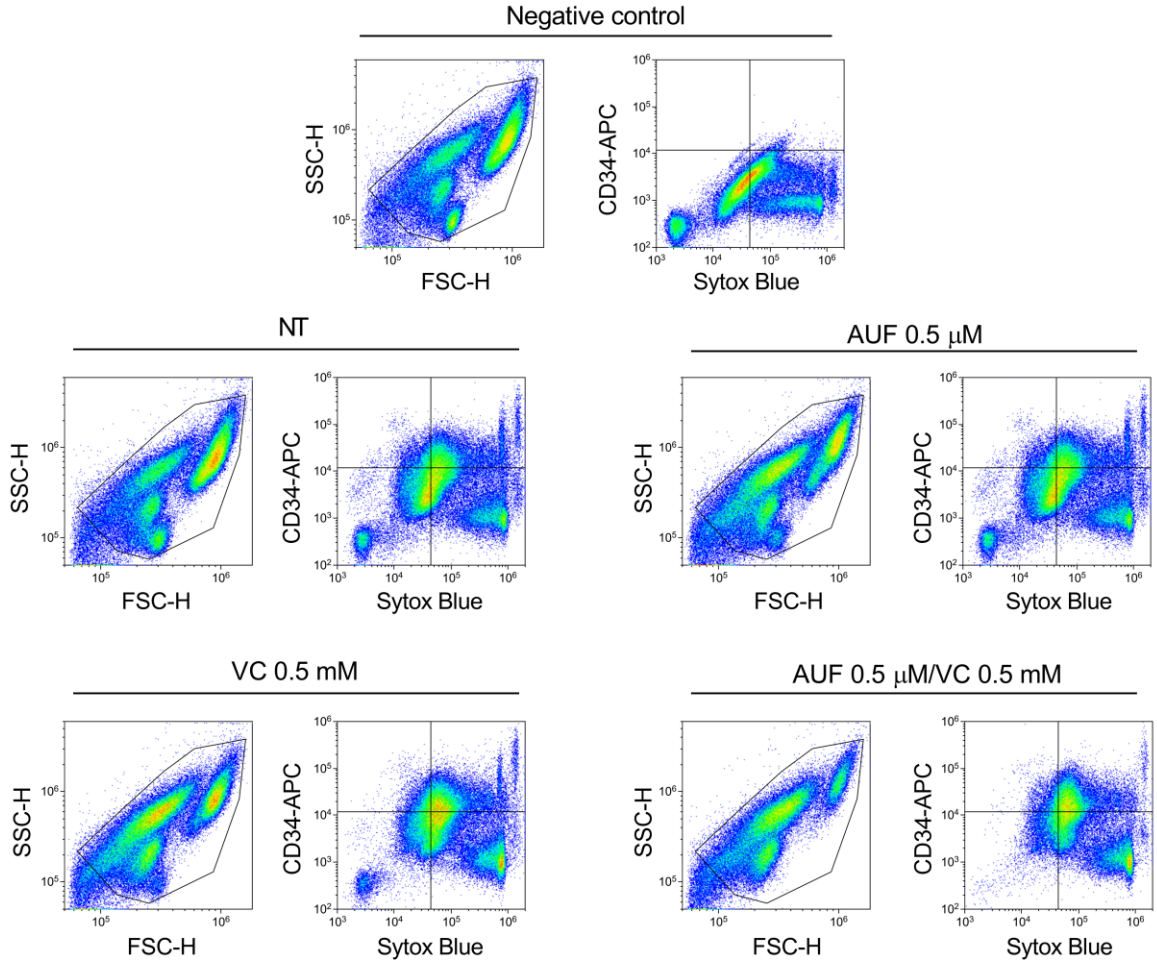

SUPPLEMENTARY FIGURE S4. Effect of AUF, VC and AUF/VC combination on AML_04 sample, measured by flow cytometry. Anti-CD34 antibody failed to identify a clear $CD34^{+}$ population, preventing evaluation of effect of treatments. NT, no drug-treated control.